

Language-Guided Transformer Tokenizer for Human Motion Generation

Sheng Yan¹Yong Wang²Xin Du²Junsong Yuan³Mengyuan Liu⁴ *¹Transsion Ltd.²Chongqing University of Technology³State University of New York at Buffalo⁴ Peking University

<https://eanson023.github.io/LG-Tok/>

Abstract

In this paper, we focus on motion discrete tokenization, which converts raw motion into compact discrete tokens—a process proven crucial for efficient motion generation. In this paradigm, increasing the number of tokens is a common approach to improving motion reconstruction quality, but more tokens make it more difficult for generative models to learn. To maintain high reconstruction quality while reducing generation complexity, we propose leveraging language to achieve efficient motion tokenization, which we term *Language-Guided Tokenization* (LG-Tok). LG-Tok aligns natural language with motion at the tokenization stage, yielding compact, high-level semantic representations. This approach not only strengthens both tokenization and detokenization but also simplifies the learning of generative models. Furthermore, existing tokenizers predominantly adopt convolutional architectures, whose local receptive fields struggle to support global language guidance. To this end, we propose a Transformer-based Tokenizer that leverages attention mechanisms to enable effective alignment between language and motion. Additionally, we design a language-drop scheme, in which language conditions are randomly removed during training, enabling the detokenizer to support language-free guidance during generation. On the HumanML3D and Motion-X generation benchmarks, LG-Tok achieves Top-1 scores of 0.542 and 0.582, outperforming state-of-the-art methods (MARDM: 0.500 and 0.528), and with FID scores of 0.057 and 0.088, respectively, versus 0.114 and 0.147. LG-Tok-mini uses only half the tokens while maintaining competitive performance (Top-1: 0.521/0.588, FID: 0.085/0.071), validating the efficiency of our semantic representations.

1. Introduction

Text-driven human motion generation [1–9] enables the synthesis of realistic human motions based on natural lan-

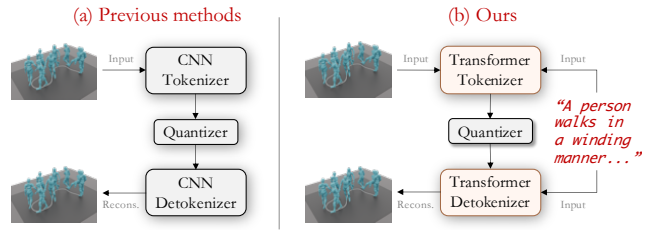


Figure 1. Comparison between previous CNN-based tokenizers and our Language-Guided Transformer Tokenizer (LG-Tok). Our method aligns language and motion during tokenization, leveraging the transformer’s flexibility.

guage descriptions, with widespread applications in game animation, virtual reality, and video motion editing, etc. In recent years, the two-stage paradigm, combining motion tokenization with generative models [10–15], has demonstrated a pivotal role in efficiently synthesizing high-fidelity motions. These methods tokenize continuous motion representations into discrete tokens, thereby enabling the direct utilization of well-established generative transformer training and sampling techniques [16–20] with minimal modifications.

As the core of this paradigm, the properties of motion tokeniza-

#Tokens	104	160	236
rFID↓	0.143	0.110	0.090
gFID↓	0.230	0.205	0.257

Table 1. Performance against #Tokens.

tion significantly influence the performance of generative transformers. Despite various motion tokenization studies focusing on improving training objectives [10, 21] or optimizing quantization [12, 22, 23], current methods still suffer from a fundamental trade-off between reconstruction and generation quality. As shown in Table 1, increasing the number of tokens typically improves motion reconstruction quality (rFID). However, the generation process exhibits a different behavior—more tokens increase learning difficulty, leading to suboptimal results (gFID). Based on this observation, we raise the question: *Can we maintain sufficient tokens for high-quality reconstruction while simultaneously reducing the learning difficulty of token sequences for generative models?*

Our key insight is that language descriptions naturally

*Corresponding author.

provide high-level semantic abstractions—*e.g.*, “*a person walks forward*” encapsulates core motion intent. Introducing language into tokenization may alleviate the semantic burden on tokens, enabling them to focus on fine-grained details that text cannot fully convey. To this end, we propose Language-Guided Tokenization (LG-Tok), which aligns natural language with motion during tokenization, aiming to provide compact, high-level semantic representations. This approach, typically reserved for the generation phase, is extended to the tokenization stage in our work. It achieves three benefits: 1) enables latent tokens to learn motion representations while simultaneously absorbing linguistic semantic knowledge during the tokenizing process; 2) allows language conditions to assist in effectively reconstructing the input motion during the detokenizing process. 3) simplifies the learning of generative models. For instance, on the Motion-X dataset [24], our compact semantic representations reduce model perplexity from 146.5 to 103.1 and improve FID from 0.257 to 0.088, indicating easier and more effective learning.

Notably, existing tokenizers [10, 12, 21, 23] predominantly adopt convolutional tokenizer-detokenizer architectures, whose local receptive fields struggle to support global language guidance. To address this, we propose a Transformer-based Tokenizer that leverages flexible attention mechanisms to enable effective alignment between language and motion, while enhancing the global contextual awareness of token representations. Specifically, we pre-define a learnable sequence of latent tokens that are concatenated with both motion and language representations. Following feature encoding by the transformer-based tokenizer, these latent tokens form semantically informed representations. After vector quantization, a transformer-based detokenizer reconstructs the input motion from the masked token sequences.

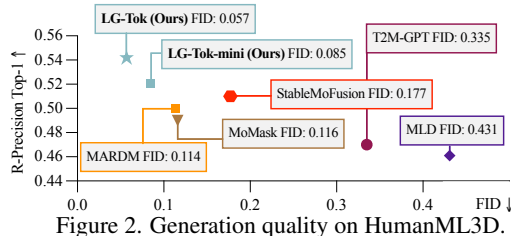


Figure 2. Generation quality on HumanML3D.

Furthermore, we design a language-drop scheme, in which language conditions are randomly removed during training. This simple yet effective strategy enables the detokenizer to support language-free guidance decoding during motion generation. Fig. 2 shows our LG-Tok outperforming representative baselines. Quantitatively, on HumanML3D [25] and Motion-X benchmarks, LG-Tok achieves Top-1 scores of **0.542** and **0.582**, outperforming state-of-the-art methods (MARDM [26]: 0.500 and 0.528), and with FID scores of **0.057** and **0.088** respectively, versus 0.114 and 0.147. LG-Tok-mini utilizes only half the

tokens while maintaining competitive performance (Top-1: 0.521/0.588, FID: 0.085/0.071), validating the efficiency of our semantic representations. In summary, our contributions are as follows:

- We propose Language-Guided Tokenization (LG-Tok), which achieves alignment between natural language and motion during the motion tokenization phase.
- We introduce a Transformer-based Tokenizer that leverages attention mechanisms to enable effective language-motion alignment and enhance global contextual awareness of token representations.
- We design a language-drop scheme that enables the detokenizer to support language-free guidance decoding during motion generation.

2. Related Work

Motion tokenization. Motion tokenizers [3, 10–12, 21, 27–30] play a crucial role in efficiently synthesizing high-fidelity motion by reducing computational costs while improving generation quality and efficiency. This has been achieved through autoencoders (AEs) [30, 31]. This general design compresses motion into low-dimensional representations, which are decoded back to the original space. Variational autoencoders (VAEs) [32, 33] extend this paradigm by introducing probability distributions, enabling stochastic sampling and generative capabilities. TEMOS [28] is a representative work, aligning a text encoder’s output distribution with the VAE’s latent space to enable text-conditioned motion generation. Latent diffusion models [34–36] further exploit compressed spaces—avoiding the cost of diffusion in the raw motion space. More recently, MARDM [26] performs masked autoregressive diffusion directly on deterministic AE latents, mitigating the sampling noise inherent to VAE representations.

Alternatively, Vector Quantized VAEs (VQ-VAE) [37] insert a quantization step between AE encoders (tokenizers) and decoders (detokenizers), replacing continuous latent distributions with discrete codes that partition the motion space into categorical units. TM2T [21] first applied VQ-VAE to motion, introducing discrete motion tokens. This discrete tokenization facilitates the use of powerful sequence-based generative models [19, 20, 38, 39]. Subsequent variants [10, 14, 40], *e.g.* RQ-VAE [12, 41] and FSQ [15, 22], further refined the quantization and enabled the integration of advanced generative architectures. In this paper, we focus on this discrete (*i.e.*, VQ-based) tokenization pipeline. Based on our observation of the fundamental trade-off between reconstruction and generation in current methods, we propose leveraging language guidance during tokenization to provide compact semantic representations, thereby maintaining high reconstruction quality while reducing the learning difficulty for generative models.

Text-driven motion generation. Natural language pro-

vides rich semantic cues for specifying actions, velocities, and directions, making it a key conditioning modality for human motion synthesis [2–9, 42]. Early GAN-based work, such as Text2Action [43], generated diverse motions from textual descriptions, while JL2P [44] employed GRU-based encoders and decoders to map text to movement. Inspired by advances in text-to-image generation, recent approaches predominantly adopt diffusion or VQ-based paradigms. Diffusion models [45–51] simulate a forward noising process and train networks to reverse it; MLD [34] improves efficiency by operating in latent space, while PhysDiff [52] enforces physical constraints during generation. VQ-based methods [13–15, 22, 40, 41, 53, 54], *e.g.*, T2M-GPT [10], quantize motion into discrete tokens via VQ-VAE and model them autoregressively using GPT-style [18, 19] transformers. MoMask [12] and MMM [11] adopt MaskGIT-style [20] masked training and non-autoregressive sampling, and MoSa [23] adapts scalable autoregressive modeling from the image domain [17]. In this paper, we adopt MoSa as our generative model given its notable gains in quality and efficiency. To demonstrate the generalizability of our approach, we also apply LG-Tok to MoMask, showing consistent improvements across different generative paradigms.

Image tokenization. Image tokenization has emerged as a fundamental technique bridging various vision tasks. This field has diverged into two main branches: understanding-oriented and generation-oriented. Understanding-oriented approaches [55–57] leverage large language models (LLMs) to create semantic representations for tasks such as classification [58] and segmentation [59]. Meanwhile, generation-oriented methods, such as VQ-GAN [60, 61], emphasize learning latent spaces for detail-preserving compression. These methods typically employ 2D latent grids with fixed downsampling factors [9, 17, 20, 62–64]. TikTok [65] first introduces a transformer-based 1D tokenizer that generates global tokens as more compact representations of images. Subsequently, numerous variants have refined it [66–69]. *e.g.*, TxtTok [70] extends this paradigm by incorporating image captions as conditions during tokenization, significantly improving reconstruction quality and compression rates. Inspired by these works, we introduce natural language guidance into motion tokenization and propose a transformer-based tokenizer to enable effective alignment. While transformer-based tokenizers have been explored in continuous VAE representations [28, 34], their application in VQ-based tokenizers remains limited—existing attempts [23, 71] only stack shallow self-attention layers after CNN-based residual blocks, which may be insufficient for effective alignment. Additionally, we design a novel language-drop scheme that enables the detokenizer to support language-free guidance decoding during motion generation.

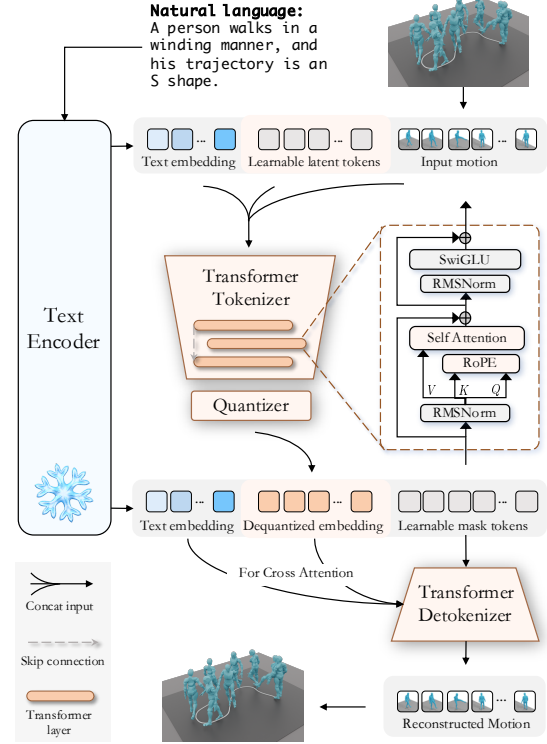


Figure 3. **Illustration of our LG-Tok framework.** Given an input motion sequence and corresponding natural language description, a frozen text encoder (*e.g.*, LLaMA [72]) extracts text embeddings which are concatenated with learnable latent tokens and motions, and fed into a Transformer-based tokenizer to produce high-level semantic motion tokens. The quantizer then quantized these tokens into discrete codes for downstream generative modeling training. During detokenization, the dequantized embeddings, learnable mask tokens, and corresponding text embeddings interact via cross-attention layers within a Transformer-based detokenizer to reconstruct the motion sequence. For generation, motion tokens sampled by the trained generative model are dequantized and fed into the detokenizer to synthesize diverse, high-fidelity human motion.

3. Method

3.1. Preliminary

Motion tokenizer. Human motion tokenization converts continuous motion representations into discrete tokens to facilitate the generative models. Traditional approaches employ vanilla VQ-VAE [10, 11, 21], where a tokenizer (encoder) $\mathcal{E}(\cdot)$ compresses motion m into latent features $z = \mathcal{E}(m) \in \mathbb{R}^{T \times d}$, followed by a quantizer $\mathcal{Q}(z)$ that maps each latent feature to its nearest codebook entry, producing discrete tokens $x \in [V]^T$, where V is the codebook size. Then, a detokenizer (decoder) $\mathcal{D}(\cdot)$ reconstructs motion from the dequantized embeddings $\hat{m} = \mathcal{D}(\hat{z})$. To address quantization errors, Residual VQ-VAE [12, 41] performs iterative residual quantization with N quantizers, cre-

ating the same-scale token sets $(x^{(1)}, \dots, x^{(N)})$ where each $x^{(n)} \in [V]^T$. Recent work, MoSa [23], introduces interpolations before each residual quantization to construct tokens at different scales $S = (s_1, s_2, \dots, s_N)$ through downsampling: $x^{(n)} = \mathcal{Q}^{(n)}(\Downarrow(z^{(n)}, s_n))$ where the symbol $\Downarrow(\cdot, s_n)$ denotes downsampling latent features to specific granularities s_n . This process produces compact multi-scale tokens $x^{(n)} \in [V]^{s_n}$ rather than same-scale representations.

Generative model. Leveraging multi-scale tokens, MoSa enables Scalable Autoregressive (SAR) modeling that reformulates traditional token-by-token prediction [10] into scale-by-scale generation. The SAR likelihood is defined as:

$$p(x^{(1)}, \dots, x^{(N)} | c) = \prod_{n=1}^N p(x^{(n)} | x^{(1)}, \dots, x^{(n-1)}, c) \quad (1)$$

where $x^{(n)} = (x_1^{(n)}, \dots, x_{s_n}^{(n)})$ represents all tokens at scale s_n , and will be predicted simultaneously at step n . This approach generates multiple tokens in parallel at each autoregressive step, conditioned on previous scales and condition c . Given this framework’s notable gains in quality and efficiency, we adopt it as our generative model. We also apply LG-Tok to MoMask to demonstrate its generalizability. The complete tokenization-generation-detokenization pipeline is detailed in the appendix.

3.2. Transformer-based Tokenizer

To facilitate understanding of our approach, we introduce our Transformer-based Tokenizer first.

Existing discrete tokenizers have achieved substantial results but still exhibit a limitation in their standard workflow: The 196-frame motion is compressed into 49 latent tokens via 1D convolutional encoding with 4x downsampling, whose local receptive fields struggle to support global language guidance and to enhance the global contextual awareness of token representations. To this end, we propose a Transformer-based Tokenizer. As depicted in Fig. 3, both our tokenizer and detokenizer are attention-based [73]. We predefine a learnable sequence of latent tokens and use these tokens for reconstruction and subsequent generation. With the self-attention mechanism, token representations can enhance global contextual awareness. After feature encoding, these latent tokens constitute a representation of motion. Specifically, we concatenate a set of learnable tokens $z_l \in \mathbb{R}^{T \times d}$ of length T with linearly transformed motion $m \in \mathbb{R}^{F \times d}$ as the input to the tokenizer, and retain only the output corresponding to the learnable latent tokens as the tokenizer output:

$$z = \mathcal{E}([z_l; m]) \quad (2)$$

subsequently, the latent tokens undergo vector quantization to obtain multi-scale discrete tokens (as mentioned in Sec. 3.1) to support subsequent SAR modeling, and yield

dequantized embeddings $\hat{z} \in \mathbb{R}^{T \times d}$. For the detokenizer, we reconstruct motion from a sequence of learnable mask tokens $\hat{m}_l \in \mathbb{R}^{F \times d}$ [39, 74]:

$$\hat{m} = \mathcal{D}(\hat{m}_l, \hat{z}) \quad (3)$$

unlike the tokenizer, the mask tokens interact with the dequantized embeddings through cross-attention. This design is inspired by object queries [75] in object detection, and we provide detailed ablations in the experimental section. At the detokenizer end, we use a linear layer to regress from mask tokens to motion space. Noteably, we do not apply patchify processing [58] to motion throughout process, since 1D motion (196 frames) incurs a significantly lower computational cost than 2D images (256×256), and this operation avoids information loss.

Our architecture is closely integrated with LLaMA, incorporating RMSNorm [76], SwiGLU activation [77], and advanced rotary position embedding (RoPE) [78]. The RoPE *base* is set to 100 to accommodate short sequence tasks. We further enhance the transformer networks of both tokenizer \mathcal{E} and detokenizer \mathcal{D} with UNet-like long skip connections for higher-fidelity motion reconstruction.

3.3. Language-Guided Tokenization

Introducing language into tokenization may alleviate the semantic burden on tokens, enabling them to focus on fine-grained details that text cannot fully convey. Building on the flexibility of our transformer-based tokenizer, we introduce Language-Guided Tokenization, which aligns natural language with motion during tokenization. This approach, typically reserved for the generation phase, is extended to the tokenization stage in our work. Given textual descriptions of motion, we use a frozen LLaMA [79] as the text encoder to extract text embeddings. These embeddings are injected into both the tokenizer and detokenizer, providing semantic guidance throughout the tokenization process. As illustrated in Fig. 3, the tokenizer input is further concatenated with linearly projected text embeddings $t \in \mathbb{R}^{W \times d}$. The Eq. 2 is updated to $z = \mathcal{E}([t; z_l; m])$, yielding compact, high-level semantic representations. For the detokenizer, the mask tokens additionally interact with text embeddings through another cross-attention: $\hat{m} = \mathcal{D}(\hat{m}_l, \hat{z}, t)$. We train LG-Tok using smooth L1 loss for motion reconstruction, without involving text reconstruction. In the generation phase, the provided text descriptions are used for both generation and detokenization. The text embeddings and the latent tokens sampled by the generative model are fed into the detokenizer to produce the final motion.

Despite its simplicity, we emphasize that this approach achieves three benefits: 1) enables latent tokens to learn motion representations while simultaneously absorbing linguistic semantic knowledge during the tokenizing process; 2) allows language conditions to assist masked token se-

quences in effectively reconstructing the input motion during the detokenizing process. 3) simplifies the learning of generative models by more compact semantic representations. We demonstrated these views in our experiments.

3.4. Language-Drop Scheme

We design a language-drop scheme in which language conditions are randomly removed during training. During training, we train LG-Tok without language guidance $t = \emptyset$ with a probability of 10%. This simple yet effective strategy enables the detokenizer to support language-free guidance decoding during motion generation. The final motion \hat{m} is computed by moving the conditional motion \hat{m}_c away from the unconditional motion \hat{m}_u with guidance scale g :

$$\hat{m} = (1 + g) \times \hat{m}_c - g \times \hat{m}_u \quad (4)$$

Similar guidance techniques[17, 80, 81] have been applied during the generation process, *e.g.*, in logits[12] or noise space [26]. In contrast, our approach performs guidance in the motion space after generation, *i.e.*, at the detokenizing stage.

4. Experiment

In this section, we present the results of our experiments. We introduce our experimental setup in Sec. 4.1. Subsequently, we compare our results with competing methods in Sec. 4.2, followed by related ablation experiments in Sec. 4.4. Finally, we provide tokenizer analysis in Sec. 4.5.

4.1. Experimental Setup

We conduct experiments on two text-to-motion benchmarks: HumanML3D [25], and the larger-scale Motion-X dataset [24]. We follow the most evaluation protocol proposed in [25, 26].

Datasets. HumanML3D dataset includes 14,616 high-quality motions paired with 44,970 text descriptions, where three different captions describe each motion. Motion-X is the larger motion-text dataset, featuring greater diversity. Following the protocol of the first dataset, we filter out motion-text pairs exceeding 200 frames, resulting in 37,751 motion sequences and 61,637 text captions. The datasets are split into training, validation, and test sets with ratios of 80%, 5%, and 15%, respectively.

For standardization, both datasets adopt the `meng67` (67-dim) representation [26], as their research uncovered the redundancy of the original 263-dim features. That is, Motion-X’s whole-body representation is also converted to `meng67`. Since most textual descriptions primarily focus on body actions, we choose to ignore finger and facial information to avoid unnecessary modal discrepancies. We provide supplementary training details for the Motion-X feature extractor in the appendix.

Evaluation metrics. We adopt the following evaluation metrics: (1) the *Frechet Inception Distance (FID)*, which assesses the overall action quality by measuring the distributional difference between the high-level features of generated and real actions; (2) *R-Precision* and *Multimodal distance*, which are used to measure the semantic consistency between the input text and the generated actions; (3) *Multi-modality*, which is used to evaluate the diversity of actions generated from the exact text. (4) *CLIP-score*, which measures the compatibility of motion-text pairs by calculating the cosine similarity.

Implementation details. We train LG-Tok using the AdamW optimizer with a batch size of 128 for 200 epochs. The learning rate is reduced from 2×10^{-4} to 2×10^{-5} at the 180th epoch. We set the gradient clipping factor to 0.01 to prevent gradient explosion. No velocity loss is employed during optimization, as the `meng67` representation is sufficiently compact. For the Transformer, we stack 9 layers for both the tokenizer and detokenizer, each with 4 heads, 256 latent dimensions, and a SwiGLU dimension of 1024. To accelerate training and reduce memory usage, we enable mixed-precision training and utilize PyTorch 2.2.0 to support flash attention. For text guidance, *LLaMA-3.2-1B* serves as our text encoder, and the maximum text length is set to 77, with more extended sequences truncated. The guidance scale g is set to 2.0 and 1.0 on the HumanML3D and Motion-X, respectively. During generation, the generative model’s configuration remains unchanged, except that PAD masks are no longer required. The generation and evaluation continue to use *CLIP-ViT-B/32* for text embedding extraction. LG-Tok training can be completed on a single RTX 4090 GPU.

Model variants. To validate the high-level semantic representations of LG-Tok, we study three variants with different token scales: LG-Tok-mini (25 tokens), LG-Tok-mid (36 tokens), and LG-Tok (49 tokens). The interpolation scales mentioned in Sec. 3.1 are set to $S = (1, 2, \dots, 25)$, $S = (2, 4, \dots, 36)$, and $S = (3, 6, \dots, 49)$ respectively. All variants use $N = 10$ scales (quantizers), resulting in 104, 160, and 236 total tokens, respectively.

4.2. Text-driven Motion Generation Comparison

Quantitative comparisons. We evaluate our approach against state-of-the-art methods. Results on HumanML3D are primarily sourced from [26], while results on Motion-X are our reimplementations based on the `meng67` representation. We provide reimplementation details in the appendix. As shown in Table 2, our LG-Tok variants outperform existing methods across multiple metrics. On HumanML3D, LG-Tok achieves the best performance with a Top-1 R-Precision of **0.542** and FID of **0.057**, surpassing the previous best method, MoSa (0.518 and 0.064, respectively). Notably, even our most compact variant, LG-

Datasets	Methods	Venues	#Tokens	R Precision \uparrow			FID \downarrow	MultiModal Dist \downarrow	MultiModality \uparrow	CLIP-score \uparrow
				Top 1	Top 2	Top 3				
Human ML3D	Real motions	-	-	0.501 \pm .002	0.696 \pm .003	0.792 \pm .002	0.000 \pm .000	3.251 \pm .010	-	0.639 \pm .001
	MotionDiffuse [46]	TPAMI' 24	-	0.450 \pm .006	0.641 \pm .005	0.753 \pm .005	0.778 \pm .005	3.490 \pm .023	3.179 \pm .046	0.606 \pm .004
	T2M-GPT [10]	CVPR' 23	49	0.470 \pm .003	0.659 \pm .002	0.758 \pm .002	0.335 \pm .003	3.505 \pm .017	2.018 \pm .053	0.607 \pm .005
	MMM [11]	CVPR' 24	49	0.487 \pm .003	0.683 \pm .003	0.782 \pm .001	0.132 \pm .004	3.359 \pm .009	1.241 \pm .073	0.635 \pm .003
	MoMask [12]	CVPR' 24	294	0.490 \pm .004	0.687 \pm .003	0.786 \pm .003	0.116 \pm .006	3.353 \pm .010	1.263 \pm .079	0.637 \pm .003
	StableMoFusion \dagger [82]	ACM MM' 24	-	0.510 \pm .002	0.710 \pm .003	0.810 \pm .003	0.177 \pm .006	3.182 \pm .009	1.969 \pm .053	0.654 \pm .001
	MARDM [26]	CVPR' 25	-	0.500 \pm .004	0.695 \pm .003	0.795 \pm .003	0.114 \pm .007	3.270 \pm .009	2.231 \pm .071	0.642 \pm .002
	MoSa \dagger [23]	Arxiv' 25	236	0.518 \pm .002	0.712 \pm .002	0.809 \pm .002	0.064 \pm .004	3.150 \pm .008	1.789 \pm .056	0.657 \pm .001
	LG-Tok-mini	-	104	0.521 \pm .003	0.715 \pm .003	0.811 \pm .003	0.085 \pm .004	3.113 \pm .001	1.728 \pm .053	0.655 \pm .001
	LG-Tok-mid	-	160	0.537 \pm .003	0.729 \pm .002	0.821 \pm .002	0.109 \pm .005	3.061 \pm .010	1.674 \pm .052	0.664 \pm .001
	LG-Tok	-	236	0.542 \pm .003	0.736 \pm .002	0.830 \pm .002	0.057 \pm .003	2.997 \pm .010	1.540 \pm .059	0.669 \pm .001
Motion- X	Real motions	-	-	0.595 \pm .002	0.787 \pm .001	0.868 \pm .001	0.000 \pm .000	3.717 \pm .007	-	0.672 \pm .000
	MotionDiffuse \dagger [46]	TPAMI' 24	-	0.559 \pm .003	0.752 \pm .002	0.839 \pm .001	0.954 \pm .014	4.167 \pm .023	2.476 \pm .098	0.660 \pm .001
	T2M-GPT \dagger [10]	CVPR' 23	49	0.470 \pm .003	0.644 \pm .002	0.735 \pm .003	1.085 \pm .032	5.488 \pm .023	12.807 \pm .405	0.622 \pm .001
	MMM \dagger [11]	CVPR' 24	49	0.424 \pm .002	0.600 \pm .002	0.695 \pm .002	2.918 \pm .036	6.098 \pm .019	2.342 \pm .193	0.607 \pm .001
	MoMask \dagger [12]	CVPR' 24	294	0.502 \pm .003	0.694 \pm .002	0.790 \pm .002	0.247 \pm .008	4.832 \pm .009	2.715 \pm .091	0.644 \pm .001
	StableMoFusion \dagger [82]	ACM MM' 24	-	0.474 \pm .003	0.682 \pm .002	0.787 \pm .002	0.213 \pm .008	4.888 \pm .014	2.985 \pm .111	0.607 \pm .001
	MARDM \dagger [26]	CVPR' 25	-	0.528 \pm .003	0.727 \pm .001	0.820 \pm .002	0.147 \pm .009	4.433 \pm .018	3.077 \pm .066	0.643 \pm .001
	MoSa \dagger [23]	Arxiv' 25	236	0.513 \pm .002	0.703 \pm .002	0.796 \pm .002	0.210 \pm .009	4.783 \pm .013	3.167 \pm .122	0.654 \pm .001
	LG-Tok-mini	-	104	0.588 \pm .002	0.776 \pm .002	0.857 \pm .002	0.071 \pm .004	3.835 \pm .012	2.235 \pm .111	0.681 \pm .001
	LG-Tok-mid	-	160	0.591 \pm .002	0.781 \pm .002	0.864 \pm .001	0.076 \pm .005	3.758 \pm .010	2.245 \pm .091	0.682 \pm .000
	LG-Tok	-	236	0.582 \pm .002	0.775 \pm .001	0.858 \pm .001	0.088 \pm .006	3.844 \pm .009	2.294 \pm .088	0.682 \pm .000

Table 2. **Quantitative evaluation on the HumanML3D and Motion-X test set.** Each experiment is evaluated 20 times, and \pm indicates a 95% confidence interval. **Blue** and **Red** indicate the best and the second best result, respectively. ‘ \dagger ’ denotes our reimplementation on the meng67 representation [26].

Tok-mini, using only 104 tokens, also maintains competitive performance (0.521 Top-1 R-Precision), validating the efficiency of our high-level semantic representations. On the larger and more diverse Motion-X dataset, our methods show substantial improvements, with LG-Tok-mid achieving the best Top-1 R-Precision of **0.591**. The consistent performance gains validate that transformer-based, language-guided tokenization effectively captures motion semantics.

Qualitative comparisons. Fig. 4 displays qualitative comparisons of our approach against StableMoFusion [82], MARDM [26], and MoSa [23] based on HumanML3D checkpoints. We randomly select several generated samples for comparison. These three examples demonstrate that LG-Tok can understand more complex semantics. *e.g.*, in the first row, our method successfully understands “*in the middle*” (competitors fail to return to the middle position). In the second row, LG-Tok synthesizes more realistic crouching postures in the “*dodges quickly*” motion. In the final row, our approach exhibits better directional awareness for “*then turns to the left*”. More dynamic results can be found on our supplementary materials.

4.3. Comparison of Discrete Tokenizers

We compare our approach against existing discrete (VQ-based) tokenizers, which are predominantly CNN-based. Table 3 demonstrates our LG-Tok consistent improvements in both reconstruction and generation stages across both

datasets. Notably, by incorporating language guidance, our compact semantic representations significantly simplify the learning of generative models. On Motion-X, text-guided LG-Tok achieves substantial generation performance gains (FID: $0.257 \rightarrow 0.088$), and the perplexity we recorded decreases from 146.5 to 103.1; similar improvements on HumanML3D ($160.6 \rightarrow 155.9$). These results confirm that incorporating language into tokenization shifts the semantic burden away from tokens, enabling them to focus on fine-grained motion details beyond the reach of text descriptions.

Furthermore, without text guidance (*i.e.*, using only transformer-based tokenization from Sec. 3.2), our method outperforms most competitors, demonstrating that our transformer-based architecture provides superior global context modeling. More importantly, we integrate LG-Tok into a representative motion tokenization–plus–generation framework, MoMask. The enhanced variant, MoMask (LG-Tok), consistently surpasses the original across all evaluation metrics, demonstrating strong generalization.

4.4. Ablation Studies

Guidance hyper-parameter. Fig. 5 demonstrates the effectiveness of our language-drop scheme (mentioned in Sec. 3.4) across different guidance scales g . The results show optimal performance at $g = 2.0$ for HumanML3D and $g = 1.0$ for Motion-X. The qualitative comparisons are provided in the appendix.

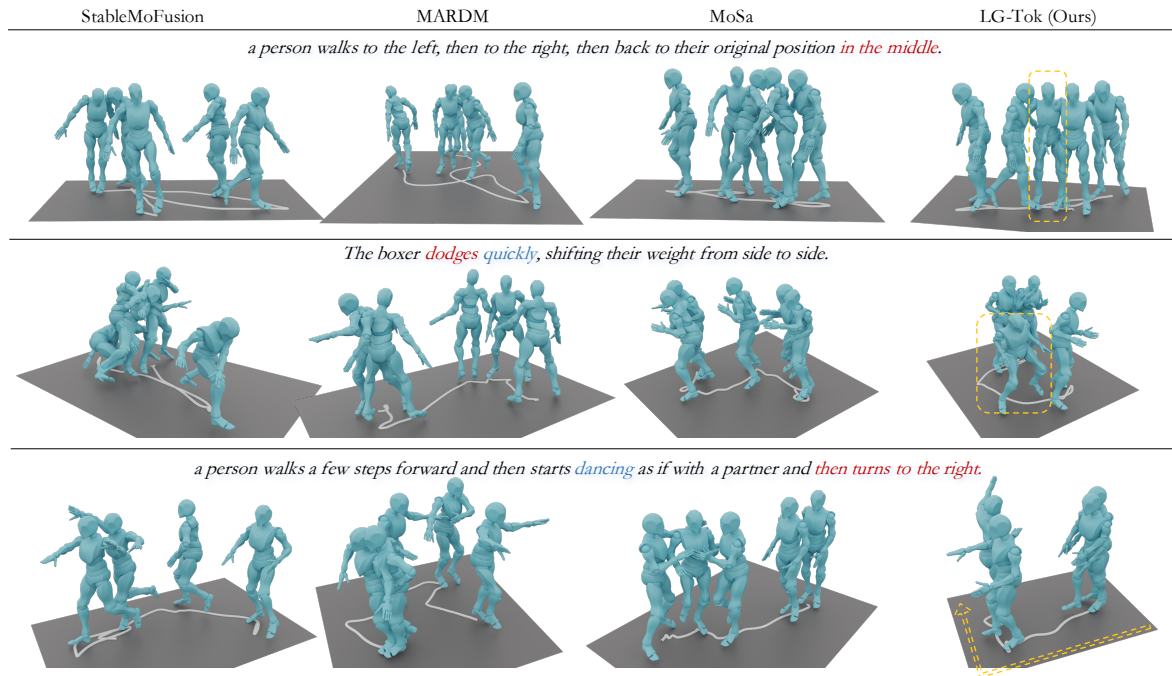


Figure 4. **Qualitative comparisons on HumanML3D dataset.** Our LG-Tok demonstrates superior semantic understanding compared to existing methods. The examples show better spatial awareness (“in the middle”), more realistic posture synthesis (“dodges quickly”), and improved directional control (“then turns to the left”).

Methods	Reconstruction			Generation	
	FID \downarrow	Top 1 \uparrow	MPJPE \downarrow	FID \downarrow	MM-Dist \downarrow
Evaluation on HumanML3D dataset					
T2M-GPT* [10]	0.081 \pm .001	0.483 \pm .003	72.6 \pm .001	0.335 \pm .003	3.505 \pm .017
MoMask* [12]	0.029 \pm .001	0.497 \pm .002	31.5 \pm .001	0.116 \pm .006	3.353 \pm .010
MoMask-reprod.	0.029 \pm .000	0.499 \pm .003	30.9 \pm .000	0.180 \pm .005	3.332 \pm .009
MoMask (LG-Tok)	0.019\pm.000	0.501 \pm .003	26.4\pm.000	0.111 \pm .005	3.300 \pm .012
MoSa [23]	0.023 \pm .000	0.496 \pm .003	43.0 \pm .000	0.064 \pm .004	3.150 \pm .008
LG-Tok	0.022 \pm .000	0.502\pm.002	39.0 \pm .000	0.057\pm.003	2.997\pm.010
w/o text guidance	0.025 \pm .000	0.494 \pm .002	39.0 \pm .000	0.062 \pm .003	3.129 \pm .008
Evaluation on Motion-X dataset					
T2M-GPT [10]	0.826 \pm .011	0.497 \pm .002	59.6 \pm .000	1.102 \pm .000	5.515 \pm .000
MoMask [12]	0.394 \pm .005	0.554 \pm .002	24.9 \pm .000	0.247 \pm .008	4.832 \pm .009
MoMask (LG-Tok)	0.076 \pm .002	0.580\pm.002	23.0\pm.000	0.157 \pm .006	4.259 \pm .008
MoSa [23]	0.072 \pm .001	0.558 \pm .002	39.0 \pm .000	0.210 \pm .009	4.783 \pm .013
LG-Tok	0.041\pm.001	0.577 \pm .002	31.0 \pm .000	0.088\pm.006	3.844\pm.009
w/o text guidance	0.090 \pm .002	0.568 \pm .002	33.0 \pm .000	0.257 \pm .010	4.274 \pm .008

Table 3. **Reconstruction and generation performance comparison.** We evaluate both reconstruction quality and generation performance across different discrete tokenizers. “w/o text guidance” denotes our approach without language guidance, *i.e.*, using only the transformer-based tokenization from Sec. 3.2. “*” denotes report from [26], and the others are our reproductions.

The remaining ablation studies were conducted on a smaller version (LG-Tok-tiny) with reduced model size and training data for efficient hyperparameter tuning. LG-Tok-tiny uses 3-layer transformers trained on 5,000 samples.

Transformer architecture. Tables 4a- 4d demonstrate the advantages of our transformer design over vanilla trans-

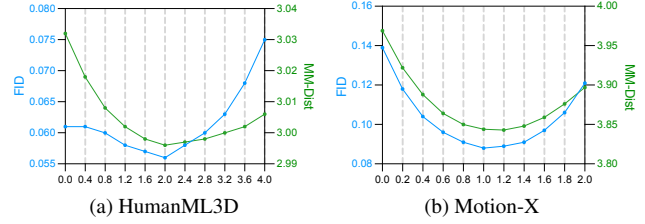


Figure 5. **Evaluation sweep over guidance scale g .** We evaluate the impact of different guidance scales on generation quality, showing optimal performance at $g = 2.0$ for HumanML3D and $g = 1.0$ for Motion-X.

formers [73]. RMSNorm, SwiGLU activation, and skip connections all contribute to improved performance. Notably, RoPE with $base=100$ is better suited for our short sequence task (\sim 10s, 196 frames) compared to other bases.

Guidance location. Table 4e validates our method’s benefits. Injecting guidance into both tokenizer and detokenizer achieves the best results, confirming that language guidance: 1) enables latent tokens to learn motion representations while simultaneously absorbing linguistic semantic knowledge during tokenizing; 2) allows language conditions to assist masked token sequences in effectively reconstructing input motion during detokenizing.

Text encoder choice. We compare popular pretrained text encoders [72, 83–85] in Table 4f. LLaMA achieves the best performance among the tested encoders.

Interaction methods. Table 4g ablates how tokens interact in both the tokenizer and detokenizer. We compare two interaction strategies: *In-context* (concatenating all tokens

Normalization	FID \downarrow	MPJPE \downarrow	Architecture	FID \downarrow	MPJPE \downarrow	Activation	FID \downarrow	MPJPE \downarrow
LayerNorm	0.050 \pm .001	58.7	GeLU	0.050 \pm .001	57.4	Skip Conn.	0.049 \pm .000	56.1
RMSNorm	0.049 \pm .000	56.1	SwiGLU	0.049 \pm .000	56.1	w/o Skip Conn.	0.059 \pm .001	61.7
(a) Normalization								
Position embedding	FID \downarrow	MPJPE \downarrow	Guidance location	FID \downarrow	MPJPE \downarrow	(c) Skip connections		
Learnable	0.065 \pm .001	54.7	None	0.064 \pm .001	64.1			
RoPE ($base=10$)	0.061 \pm .001	54.8	Tokenizer only	0.063 \pm .001	57.5			
RoPE ($base=100$)	0.049 \pm .000	56.1	Detokenizer only	0.055 \pm .000	58.7			
RoPE ($base=1000$)	0.042 \pm .001	56.3	Tokenizer & Detokenizer	0.049 \pm .000	56.1			
RoPE ($base=10000$)	0.052 \pm .001	56.6						
(d) Position embedding								
Frozen text encoder	FID \downarrow	MPJPE \downarrow	Tokenizer	Detokenizer		(e) Guidance location		
CLIP	0.051 \pm .000	59.1	In-Context	Cross-Attn.		In-Context	Cross-Attn.	
T5	0.053 \pm .000	58.9	✓	✗		✓	✗	
BERT	0.055 \pm .001	58.9	✗	✓		✗	✓	
LLaMA	0.049 \pm .000	56.1	✓	✗		✗	✓	
(f) Text encoder chosen								
(g) Latent-tokens/motion/text interaction in tokenizer & Mask-tokens/latent/text interaction in detokenizer								

Table 4. **Ablation studies on LG-Tok-tiny.** We ablate key design choices affecting LG-Tok’s reconstruction performance on HumanML3D dataset. Default setting: RMSNorm, SwiGLU activation, skip connections, RoPE with $base=100$, LLaMA text encoder, with in-context conditioning for tokenizer and cross-attention for detokenizer. Injecting natural language to both tokenizer and detokenizer obtains the best results.

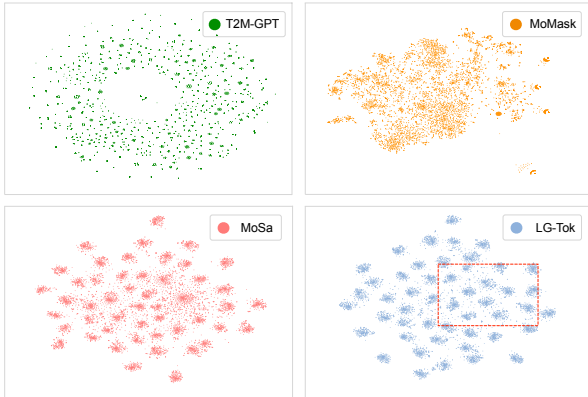


Figure 6. **t-SNE visualization of dequantized embedding space representations.** LG-Tok demonstrates well-structured clusters with clear boundaries, indicating effective capture of distinct motion patterns.

for joint self-attention) and *Cross-attention* (two separate cross-attention between different token types). The results show that In-context concatenation performs better in the tokenizer, while cross-attention excels in the detokenizer.

4.5. Tokenizer Analysis

We provide further analysis of the learned representations of our tokenizer. Fig. 6 visualizes the t-SNE representations of dequantized embeddings from different discrete tokenizers. Our LG-Tok demonstrates well-structured clusters with clear boundaries (e.g., in the red box), indicating that our compact, high-level semantic representations effectively capture distinct motion patterns. Fig. 7 compares codebook usage frequencies across different scales on the HumanML3D test-set. LG-Tok achieves more uniform

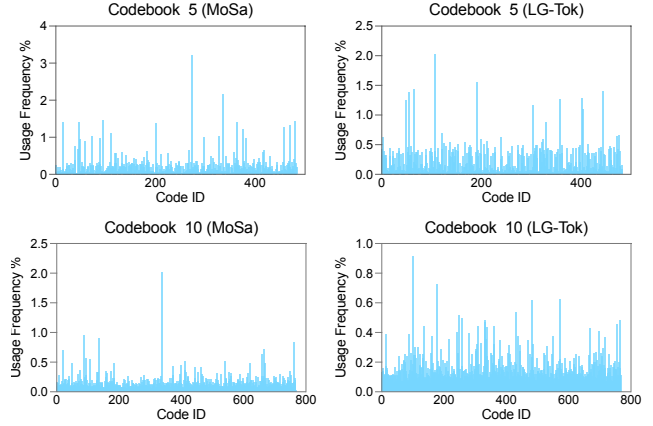


Figure 7. **Code usage comparison on the HumanML3D test-set.** LG-Tok achieves more uniform codebook utilization.

codebook utilization across all scales, indicating better coverage of the motion space. This uniform usage demonstrates that our language-guided, transformer-based approach possesses learned comprehensive motion representations without redundancy.

5. Conclusion

In this paper, we present Language-Guided Transformer Tokenization (LG-Tok) for text-driven human motion generation. By aligning natural language with motion during tokenization and employing a Transformer-based tokenizer-detokenizer architecture, LG-Tok provides semantically informed latent representations that improve reconstruction fidelity and simplify generative learning. LG-Tok achieves state-of-the-art results on HumanML3D and Motion-X benchmarks.

References

- [1] Wentao Zhu, Xiaoxuan Ma, Dongwoo Ro, Hai Ci, Jinlu Zhang, Jiaxin Shi, Feng Gao, Qi Tian, and Yizhou Wang. Human motion generation: A survey. *IEEE Transactions on Pattern Analysis and Machine Intelligence*, 2023. 1
- [2] Mathis Petrovich, Michael J Black, and Gü̈l Varol. Action-conditioned 3d human motion synthesis with transformer vae. In *Proceedings of the IEEE/CVF International Conference on Computer Vision*, pages 10985–10995, 2021. 3
- [3] Chuan Guo, Xinxin Zuo, Sen Wang, Shihao Zou, Qingyao Sun, Annan Deng, Minglun Gong, and Li Cheng. Action2motion: Conditioned generation of 3d human motions. In *Proceedings of the 28th ACM International Conference on Multimedia*, pages 2021–2029, 2020. 2
- [4] Anindita Ghosh, Noshaba Cheema, Cennet Oguz, Christian Theobalt, and Philipp Slusallek. Synthesis of compositional animations from textual descriptions. In *Proceedings of the IEEE/CVF international conference on computer vision*, pages 1396–1406, 2021.
- [5] Taoran Tang, Jia Jia, and Hanyang Mao. Dance with melody: An lstm-autoencoder approach to music-oriented dance synthesis. In *Proceedings of the 26th ACM international conference on Multimedia*, pages 1598–1606, 2018.
- [6] Nhat Le, Thang Pham, Tuong Do, Erman Tjiputra, Quang D Tran, and Anh Nguyen. Music-driven group choreography. In *Proceedings of the IEEE/CVF Conference on Computer Vision and Pattern Recognition*, pages 8673–8682, 2023.
- [7] Shiry Ginosar, Amir Bar, Gefen Kohavi, Caroline Chan, Andrew Owens, and Jitendra Malik. Learning individual styles of conversational gesture. In *Proceedings of the IEEE/CVF conference on computer vision and pattern recognition*, pages 3497–3506, 2019.
- [8] Simon Alexanderson, Rajmund Nagy, Jonas Beskow, and Gustav Eje Henter. Listen, denoise, action! audio-driven motion synthesis with diffusion models. *ACM Transactions on Graphics (TOG)*, 42(4):1–20, 2023.
- [9] Lingting Zhu, Xian Liu, Xuanyu Liu, Rui Qian, Ziwei Liu, and Lequan Yu. Taming diffusion models for audio-driven co-speech gesture generation. In *Proceedings of the IEEE/CVF Conference on Computer Vision and Pattern Recognition*, pages 10544–10553, 2023. 1, 3
- [10] Jianrong Zhang, Yangsong Zhang, Xiaodong Cun, Yong Zhang, Hongwei Zhao, Hongtao Lu, Xi Shen, and Ying Shan. Generating human motion from textual descriptions with discrete representations. In *Proceedings of the IEEE/CVF conference on computer vision and pattern recognition*, pages 14730–14740, 2023. 1, 2, 3, 4, 6, 7, 8
- [11] Ekkasit Pinyoanuntapong, Pu Wang, Minwoo Lee, and Chen Chen. Mmm: Generative masked motion model. In *Proceedings of the IEEE/CVF Conference on Computer Vision and Pattern Recognition*, pages 1546–1555, 2024. 3, 6, 8
- [12] Chuan Guo, Yuxuan Mu, Muhammad Gohar Javed, Sen Wang, and Li Cheng. Momask: Generative masked modeling of 3d human motions. In *Proceedings of the IEEE/CVF Conference on Computer Vision and Pattern Recognition*, pages 1900–1910, 2024. 1, 2, 3, 5, 6, 7, 8
- [13] Weihao Yuan, Yisheng He, Weichao Shen, Yuan Dong, Xiaodong Gu, Zilong Dong, Liefeng Bo, and Qixing Huang. Mogents: Motion generation based on spatial-temporal joint modeling. *Advances in Neural Information Processing Systems*, 37:130739–130763, 2024. 3
- [14] Zeyu Zhang, Yiran Wang, Wei Mao, Danning Li, Rui Zhao, Biao Wu, Zirui Song, Bohan Zhuang, Ian Reid, and Richard Hartley. Motion anything: Any to motion generation. *arXiv preprint arXiv:2503.06955*, 2025. 2
- [15] Zan Wang, Jingze Zhang, Yixin Chen, Baoxiong Jia, Wei Liang, and Siyuan Huang. Spatial-temporal multi-scale quantization for flexible motion generation. *arXiv preprint arXiv:2508.08991*, 2025. 1, 2, 3
- [16] Tianhong Li, Yonglong Tian, He Li, Mingyang Deng, and Kaiming He. Autoregressive image generation without vector quantization. *Advances in Neural Information Processing Systems*, 37:56424–56445, 2024. 1
- [17] Keyu Tian, Yi Jiang, Zehuan Yuan, Bingyue Peng, and Liwei Wang. Visual autoregressive modeling: Scalable image generation via next-scale prediction. *arXiv preprint arXiv:2404.02905*, 2024. 3, 5
- [18] Tom Brown, Benjamin Mann, Nick Ryder, Melanie Subbiah, Jared D Kaplan, Prafulla Dhariwal, Arvind Neelakantan, Pranav Shyam, Girish Sastry, Amanda Askell, et al. Language models are few-shot learners. *Advances in neural information processing systems*, 33:1877–1901, 2020. 3
- [19] Alec Radford, Jeffrey Wu, Rewon Child, David Luan, Dario Amodei, Ilya Sutskever, et al. Language models are unsupervised multitask learners. *OpenAI blog*, 1(8):9, 2019. 2, 3
- [20] Huiwen Chang, Han Zhang, Lu Jiang, Ce Liu, and William T Freeman. Maskgit: Masked generative image transformer. In *Proceedings of the IEEE/CVF Conference on Computer Vision and Pattern Recognition*, pages 11315–11325, 2022. 1, 2, 3
- [21] Chuan Guo, Xinxin Zuo, Sen Wang, and Li Cheng. Tm2t: Stochastic and tokenized modeling for the reciprocal generation of 3d human motions and texts. In *European Conference on Computer Vision*, pages 580–597. Springer, 2022. 1, 2, 3
- [22] Shunlin Lu, Jingbo Wang, Zeyu Lu, Ling-Hao Chen, Wenxun Dai, Junting Dong, Zhiyang Dou, Bo Dai, and Ruimao Zhang. Scamo: Exploring the scaling law in autoregressive motion generation model. In *Proceedings of the Computer Vision and Pattern Recognition Conference*, pages 27872–27882, 2025. 1, 2, 3
- [23] Mengyuan Liu, Sheng Yan, Yong Wang, Yingjie Li, Gui-Bin Bian, and Hong Liu. Mosa: Motion generation with scalable autoregressive modeling. *arXiv preprint arXiv:2511.01200*, 2025. 1, 2, 3, 4, 6, 7, 8
- [24] Jing Lin, Ailing Zeng, Shunlin Lu, Yuanhao Cai, Ruimao Zhang, Haoqian Wang, and Lei Zhang. Motion-x: A large-scale 3d expressive whole-body human motion dataset. *Advances in Neural Information Processing Systems*, 36:25268–25280, 2023. 2, 5
- [25] Chuan Guo, Shihao Zou, Xinxin Zuo, Sen Wang, Wei Ji, Xingyu Li, and Li Cheng. Generating diverse and natural 3d human motions from text. In *Proceedings of the IEEE/CVF Conference on Computer Vision and Pattern Recognition*, pages 11315–11325, 2022. 1, 2, 3

- Conference on Computer Vision and Pattern Recognition*, pages 5152–5161, 2022. 2, 5, 4
- [26] Zichong Meng, Yiming Xie, Xiaogang Peng, Zeyu Han, and Huaizu Jiang. Rethinking diffusion for text-driven human motion generation: Redundant representations, evaluation, and masked autoregression. In *Proceedings of the Computer Vision and Pattern Recognition Conference*, pages 27859–27871, 2025. 2, 5, 6, 7, 4, 8
- [27] Ekkasit Pinyanuntapong, Muhammad Usama Saleem, Pu Wang, Minwoo Lee, Sriyan Das, and Chen Chen. Bamm: Bidirectional autoregressive motion model. In *European Conference on Computer Vision*, pages 172–190. Springer, 2024. 2
- [28] Mathis Petrovich, Michael J Black, and GüL Varol. Temos: Generating diverse human motions from textual descriptions. In *European Conference on Computer Vision*, pages 480–497. Springer, 2022. 2, 3
- [29] Qi Wu, Yubo Zhao, Yifan Wang, Yu-Wing Tai, and Chi-Keung Tang. Motionllm: Multimodal motion-language learning with large language models. *arXiv e-prints*, pages arXiv–2405, 2024.
- [30] Taku Komura, Ikhsanul Habibie, Daniel Holden, Jonathan Schwarz, and Joe Yearsley. A recurrent variational autoencoder for human motion synthesis. In *The 28th British Machine Vision Conference*, 2017. 2
- [31] Guy Tevet, Brian Gordon, Amir Hertz, Amit H Bermano, and Daniel Cohen-Or. Motionclip: Exposing human motion generation to clip space. In *European Conference on Computer Vision*, pages 358–374. Springer, 2022. 2, 4
- [32] Diederik P Kingma and Max Welling. Auto-encoding variational bayes. *arXiv preprint arXiv:1312.6114*, 2013. 2
- [33] Diederik P Kingma, Max Welling, et al. An introduction to variational autoencoders. *Foundations and Trends® in Machine Learning*, 12(4):307–392, 2019. 2
- [34] Xin Chen, Biao Jiang, Wen Liu, Zilong Huang, Bin Fu, Tao Chen, and Gang Yu. Executing your commands via motion diffusion in latent space. In *Proceedings of the IEEE/CVF Conference on Computer Vision and Pattern Recognition*, pages 18000–18010, 2023. 2, 3
- [35] Nefeli Andreou, Xi Wang, Victoria Fernández Abrevaya, Marie-Paule Cani, Yiorgos Chrysanthou, and Vicky Kalogeiton. Lead: Latent realignment for human motion diffusion. In *Computer Graphics Forum*, page e70093. Wiley Online Library, 2025.
- [36] Samaneh Azadi, Akbar Shah, Thomas Hayes, Devi Parikh, and Sonal Gupta. Make-an-animation: Large-scale text-conditional 3d human motion generation. In *Proceedings of the IEEE/CVF International Conference on Computer Vision*, pages 15039–15048, 2023. 2
- [37] Aaron Van Den Oord, Oriol Vinyals, et al. Neural discrete representation learning. *Advances in neural information processing systems*, 30, 2017. 2
- [38] Dzmitry Bahdanau, Kyunghyun Cho, and Yoshua Bengio. Neural machine translation by jointly learning to align and translate. *arXiv preprint arXiv:1409.0473*, 2014. 2
- [39] Jacob Devlin, Ming-Wei Chang, Kenton Lee, and Kristina Toutanova. Bert: Pre-training of deep bidirectional transformers for language understanding. In *Proceedings of the 2019 conference of the North American chapter of the association for computational linguistics: human language technologies, volume 1 (long and short papers)*, pages 4171–4186, 2019. 2, 4
- [40] Junyu Shi, Lijiang Liu, Yong Sun, Zhiyuan Zhang, Jinni Zhou, and Qiang Nie. Genm3: Generative pretrained multi-path motion model for text conditional human motion generation. *arXiv preprint arXiv:2503.14919*, 2025. 2, 3
- [41] Zeyu Zhang, Hang Gao, Akide Liu, Qi Chen, Feng Chen, Yiran Wang, Danning Li, Rui Zhao, Zhenming Li, Zhongwen Zhou, et al. Kmm: Key frame mask mamba for extended motion generation. *arXiv preprint arXiv:2411.06481*, 2024. 2, 3
- [42] Yuanhao Zhai, Mingzhen Huang, Tianyu Luan, Lu Dong, Ifeoma Nwogu, Siwei Lyu, David Doermann, and Junsong Yuan. Language-guided human motion synthesis with atomic actions. In *Proceedings of the 31st ACM International Conference on Multimedia*, pages 5262–5271, 2023. 3
- [43] Hyemin Ahn, Timothy Ha, Yunho Choi, Hwiyeon Yoo, and Songhwai Oh. Text2action: Generative adversarial synthesis from language to action. In *2018 IEEE International Conference on Robotics and Automation (ICRA)*, pages 5915–5920. IEEE, 2018. 3
- [44] Chaitanya Ahuja and Louis-Philippe Morency. Language2pose: Natural language grounded pose forecasting. In *2019 International Conference on 3D Vision (3DV)*, pages 719–728. IEEE, 2019. 3
- [45] Mingyuan Zhang, Xinying Guo, Liang Pan, Zhongang Cai, Fangzhou Hong, Huirong Li, Lei Yang, and Ziwei Liu. Remodiffuse: Retrieval-augmented motion diffusion model. In *Proceedings of the IEEE/CVF International Conference on Computer Vision*, pages 364–373, 2023. 3
- [46] Mingyuan Zhang, Zhongang Cai, Liang Pan, Fangzhou Hong, Xinying Guo, Lei Yang, and Ziwei Liu. Motiondiffuse: Text-driven human motion generation with diffusion model. *arXiv preprint arXiv:2208.15001*, 2022. 6, 8
- [47] Korrawe Karunratanakul, Konpat Preechakul, Supasorn Suwajanakorn, and Siyu Tang. Guided motion diffusion for controllable human motion synthesis. In *Proceedings of the IEEE/CVF International Conference on Computer Vision*, pages 2151–2162, 2023.
- [48] Wenyang Zhou, Zhiyang Dou, Zeyu Cao, Zhouyingcheng Liao, Jingbo Wang, Wenjia Wang, Yuan Liu, Taku Komura, Wenping Wang, and Lingjie Liu. Emdm: Efficient motion diffusion model for fast and high-quality motion generation. In *European Conference on Computer Vision*, pages 18–38. Springer, 2024.
- [49] Jihoon Kim, Jiseob Kim, and Sungjoon Choi. Flame: Free-form language-based motion synthesis & editing. In *Proceedings of the AAAI Conference on Artificial Intelligence*, volume 37, pages 8255–8263, 2023.
- [50] Weilin Wan, Yiming Huang, Shutong Wu, Taku Komura, Wenping Wang, Dinesh Jayaraman, and Lingjie Liu. Diffusionphase: Motion diffusion in frequency domain. *arXiv preprint arXiv:2312.04036*, 2023.
- [51] Yunhong Lou, Linchao Zhu, Yaxiong Wang, Xiaohan Wang, and Yi Yang. Diversemotion: Towards diverse human

- motion generation via discrete diffusion. *arXiv preprint arXiv:2309.01372*, 2023. 3
- [52] Ye Yuan, Jiaming Song, Umar Iqbal, Arash Vahdat, and Jan Kautz. Physdiff: Physics-guided human motion diffusion model. In *Proceedings of the IEEE/CVF international conference on computer vision*, pages 16010–16021, 2023. 3
- [53] Chongyang Zhong, Lei Hu, Zihao Zhang, and Shihong Xia. Att2m: Text-driven human motion generation with multi-perspective attention mechanism. In *Proceedings of the IEEE/CVF international conference on computer vision*, pages 509–519, 2023. 3
- [54] Zhe Li, Weihao Yuan, Yisheng He, Lingteng Qiu, Shenhao Zhu, Xiaodong Gu, Weichao Shen, Yuan Dong, Zilong Dong, and Laurence T Yang. Lamp: Language-motion pretraining for motion generation, retrieval, and captioning. *arXiv preprint arXiv:2410.07093*, 2024. 3
- [55] Chuofan Ma, Yi Jiang, Junfeng Wu, Jihan Yang, Xin Yu, Ze-huan Yuan, Bingyue Peng, and Xiaojuan Qi. Unitok: A unified tokenizer for visual generation and understanding. *arXiv preprint arXiv:2502.20321*, 2025. 3
- [56] Junnan Li, Dongxu Li, Silvio Savarese, and Steven Hoi. Blip-2: Bootstrapping language-image pre-training with frozen image encoders and large language models. In *International conference on machine learning*, pages 19730–19742. PMLR, 2023.
- [57] Jean-Baptiste Alayrac, Jeff Donahue, Pauline Luc, Antoine Miech, Iain Barr, Yana Hasson, Karel Lenc, Arthur Mensch, Katherine Millican, Malcolm Reynolds, et al. Flamingo: a visual language model for few-shot learning. *Advances in neural information processing systems*, 35:23716–23736, 2022. 3
- [58] Alexey Dosovitskiy, Lucas Beyer, Alexander Kolesnikov, Dirk Weissenborn, Xiaohua Zhai, Thomas Unterthiner, Mostafa Dehghani, Matthias Minderer, Georg Heigold, Sylvain Gelly, et al. An image is worth 16x16 words: Transformers for image recognition at scale. *arXiv preprint arXiv:2010.11929*, 2020. 3, 4
- [59] Huiyu Wang, Yukun Zhu, Hartwig Adam, Alan Yuille, and Liang-Chieh Chen. Max-deeplab: End-to-end panoptic segmentation with mask transformers. In *Proceedings of the IEEE/CVF conference on computer vision and pattern recognition*, pages 5463–5474, 2021. 3
- [60] Patrick Esser, Robin Rombach, and Bjorn Ommer. Taming transformers for high-resolution image synthesis. In *Proceedings of the IEEE/CVF conference on computer vision and pattern recognition*, pages 12873–12883, 2021. 3
- [61] Ali Razavi, Aaron Van den Oord, and Oriol Vinyals. Generating diverse high-fidelity images with vq-vae-2. *Advances in neural information processing systems*, 32, 2019. 3
- [62] Doyup Lee, Chiheon Kim, Saehoon Kim, Minsu Cho, and Wook-Shin Han. Autoregressive image generation using residual quantization. In *Proceedings of the IEEE/CVF conference on computer vision and pattern recognition*, pages 11523–11532, 2022. 3
- [63] Xiang Li, Kai Qiu, Hao Chen, Jason Kuen, Jiuxiang Gu, Bhiksha Raj, and Zhe Lin. Imagefolder: Autoregressive image generation with folded tokens. *arXiv preprint arXiv:2410.01756*, 2024.
- [64] Kai Qiu, Xiang Li, Jason Kuen, Hao Chen, Xiaohao Xu, Jiuxiang Gu, Yinyi Luo, Bhiksha Raj, Zhe Lin, and Marios Savvides. Robust latent matters: Boosting image generation with sampling error synthesis. *arXiv preprint arXiv:2503.08354*, 2025. 3
- [65] Qihang Yu, Mark Weber, Xueqing Deng, Xiaohui Shen, Daniel Cremers, and Liang-Chieh Chen. An image is worth 32 tokens for reconstruction and generation. *Advances in Neural Information Processing Systems*, 37:128940–128966, 2024. 3
- [66] Pingyu Wu, Kai Zhu, Yu Liu, Longxiang Tang, Jian Yang, Yansong Peng, Wei Zhai, Yang Cao, and Zheng-Jun Zha. Alitok: Towards sequence modeling alignment between tokenizer and autoregressive model. *arXiv preprint arXiv:2506.05289*, 2025. 3
- [67] Hao Chen, Ze Wang, Xiang Li, Ximeng Sun, Fangyi Chen, Jiang Liu, Jindong Wang, Bhiksha Raj, Zicheng Liu, and Emad Barsoum. Softvq-vae: Efficient 1-dimensional continuous tokenizer. In *Proceedings of the Computer Vision and Pattern Recognition Conference*, pages 28358–28370, 2025.
- [68] Lei Zhu, Fangyun Wei, Yanye Lu, and Dong Chen. Scaling the codebook size of vq-gan to 100,000 with a utilization rate of 99%. *Advances in Neural Information Processing Systems*, 37:12612–12635, 2024.
- [69] Jiawei Yang, Tianhong Li, Lijie Fan, Yonglong Tian, and Yue Wang. Latent denoising makes good visual tokenizers. *arXiv preprint arXiv:2507.15856*, 2025. 3
- [70] Kaiwen Zha, Lijun Yu, Alireza Fathi, David A Ross, Cordelia Schmid, Dina Katabi, and Xiuye Gu. Language-guided image tokenization for generation. In *Proceedings of the Computer Vision and Pattern Recognition Conference*, pages 15713–15722, 2025. 3
- [71] Chuan Guo, Inwoo Hwang, Jian Wang, and Bing Zhou. Snapmogen: Human motion generation from expressive texts. *arXiv preprint arXiv:2507.09122*, 2025. 3
- [72] Abhimanyu Dubey, Abhinav Jauhri, Abhinav Pandey, Abhishek Kadian, Ahmad Al-Dahle, Aiesha Letman, Akhil Mathur, Alan Schelten, Amy Yang, Angela Fan, et al. The llama 3 herd of models. *arXiv e-prints*, pages arXiv–2407, 2024. 3, 7
- [73] Ashish Vaswani, Noam Shazeer, Niki Parmar, Jakob Uszkoreit, Llion Jones, Aidan N Gomez, Łukasz Kaiser, and Illia Polosukhin. Attention is all you need. *Advances in neural information processing systems*, 30, 2017. 4, 7
- [74] Kaiming He, Xinlei Chen, Saining Xie, Yanghao Li, Piotr Dollár, and Ross Girshick. Masked autoencoders are scalable vision learners. In *Proceedings of the IEEE/CVF conference on computer vision and pattern recognition*, pages 16000–16009, 2022. 4
- [75] Nicolas Carion, Francisco Massa, Gabriel Synnaeve, Nicolas Usunier, Alexander Kirillov, and Sergey Zagoruyko. End-to-end object detection with transformers. In *European conference on computer vision*, pages 213–229. Springer, 2020. 4
- [76] Biao Zhang and Rico Sennrich. Root mean square layer normalization. *Advances in neural information processing systems*, 32, 2019. 4
- [77] Noam Shazeer. Glu variants improve transformer. *arXiv preprint arXiv:2002.05202*, 2020. 4

- [78] Jianlin Su, Murtadha Ahmed, Yu Lu, Shengfeng Pan, Wen Bo, and Yunfeng Liu. Roformer: Enhanced transformer with rotary position embedding. *Neurocomputing*, 568:127063, 2024. 4
- [79] Aaron Grattafiori, Abhimanyu Dubey, Abhinav Jauhri, Abhinav Pandey, Abhishek Kadian, Ahmad Al-Dahle, Aiesha Letman, Akhil Mathur, Alan Schelten, Alex Vaughan, et al. The llama 3 herd of models. *arXiv preprint arXiv:2407.21783*, 2024. 4
- [80] Jonathan Ho and Tim Salimans. Classifier-free diffusion guidance. *arXiv preprint arXiv:2207.12598*, 2022. 5
- [81] Alexander Quinn Nichol and Prafulla Dhariwal. Improved denoising diffusion probabilistic models. In *International conference on machine learning*, pages 8162–8171. PMLR, 2021. 5
- [82] Yiheng Huang, Hui Yang, Chuanchen Luo, Yuxi Wang, Shibiao Xu, Zhaoxiang Zhang, Man Zhang, and Junran Peng. Stablemofusion: Towards robust and efficient diffusion-based motion generation framework. In *Proceedings of the 32nd ACM International Conference on Multimedia*, pages 224–232, 2024. 6, 8
- [83] Benjamin Warner, Antoine Chaffin, Benjamin Clavié, Orion Weller, Oskar Hallström, Said Taghadouini, Alexis Gallagher, Raja Biswas, Faisal Ladhak, Tom Aarsen, et al. Smarter, better, faster, longer: A modern bidirectional encoder for fast, memory efficient, and long context finetuning and inference. *arXiv preprint arXiv:2412.13663*, 2024. 7
- [84] Hyung Won Chung, Le Hou, Shayne Longpre, Barret Zoph, Yi Tay, William Fedus, Yunxuan Li, Xuezhi Wang, Mostafa Dehghani, Siddhartha Brahma, et al. Scaling instruction-finetuned language models. *Journal of Machine Learning Research*, 25(70):1–53, 2024.
- [85] Alec Radford, Jong Wook Kim, Chris Hallacy, Aditya Ramesh, Gabriel Goh, Sandhini Agarwal, Girish Sastry, Amanda Askell, Pamela Mishkin, Jack Clark, et al. Learning transferable visual models from natural language supervision. In *International conference on machine learning*, pages 8748–8763. PMLR, 2021. 7
- [86] Sheng Yan, Yang Liu, Haoqiang Wang, Xin Du, Mengyuan Liu, and Hong Liu. Cross-modal retrieval for motion and text via droptriple loss. In *Proceedings of the 5th ACM International Conference on Multimedia in Asia*, pages 1–7, 2023. 4
- [87] Mathis Petrovich, Michael J Black, and Gü̈l Varol. Tmr: Text-to-motion retrieval using contrastive 3d human motion synthesis. In *Proceedings of the IEEE/CVF International Conference on Computer Vision*, pages 9488–9497, 2023. 4

Language-Guided Transformer Tokenizer for Human Motion Generation

Supplementary Material

A. Overview

The supplementary material is organized into the following sections:

- Section [B](#): Complete tokenization-generation-detokenization pipeline
- Section [C](#): Robust language guidance
- Section [D](#): Feature extractor training on the Motion-X dataset
- Section [E](#): Details of baseline reproduction on the Motion-X dataset
- Section [F](#): Qualitative comparison for text guidance
- Section [G](#): The role of language guidance in the detokenization stage during generation
- Section [H](#): More qualitative results
- Section [I](#): Application: motion editing
- Section [J](#): Evaluation of average inference time
- Section [K](#): Limitations

B. Complete Tokenization-Generation-Detokenization Pipeline

In this section, we present the complete tokenization-generation-detokenization pipeline to facilitate a comprehensive understanding of the interplay between tokenization and generation. We adopt the Scalable AutoRegressive (SAR) modeling framework, MoSa [23], as our generative model, benefiting from its notable performance gains. As illustrated in Fig. 8, we apply multi-scale quantization in (a) *Language-Guided Motion Tokenization*, where the retained multi-scale token sets enable (b) *Scalable AutoRegressive (SAR) Modeling*. In the SAR section, we demonstrate the training procedure. Finally, we illustrate how the trained LG-Tok and SAR models interact to generate high-quality, diverse motions conditioned on natural language descriptions. We elaborate on this pipeline through three stages:

1) LG-Tok Training Stage. The orange dashed line illustrates the tokenization flow. Since the tokenization process is detailed in Sec. 3, we focus on constructing the multi-scale quantizer. Unlike standard residual quantization, the multi-scale quantizer introduces a downsample-quantize-upsample interpolation at each residual quantization layer, enabling the model to obtain token representations at different temporal resolutions, all of which are retained for SAR modeling in stage 2). Mathematically, the resulting multi-scale token set is denoted as:

$$x = \left\{ \underbrace{(x_1^{(1)}, \dots, x_{s_1}^{(1)}), (x_1^{(2)}, x_2^{(2)}, \dots, x_{s_2}^{(2)}), \dots, (x_1^{(N)}, x_2^{(N)}, \dots, x_{s_N}^{(N)})}_{x^{(1)}} \right\} \quad (5)$$

where $x^{(n)} \in \mathbb{R}^{s_n}$ denotes the token sequence at the n -th scale, with length controlled by a predefined scale scheduler $S = (s_1, \dots, s_N)$. For instance, in LG-Tok-mid, $S = (2, 4, \dots, 36)$ increases progressively from the coarsest scale (2 tokens) to the finest scale (36 tokens).

We now describe how multi-scale tokens are obtained through the quantization process. After feature encoding by the tokenizer, the latent features $z \in \mathbb{R}^{T \times d}$ sequentially pass through N sequential quantizer layers \mathcal{Q} . At each layer, A downsampling operation $\Downarrow(\cdot, s_n)$ is first applied to reduce the latent features $z^{(n)}$ to the target scale s_n . The downsampled features are then quantized by retrieving their nearest codebook entries, generating the n -th scale tokens (discrete codes) $x^{(n)} = \mathcal{Q}^{(n)}(\Downarrow(z^{(n)}, s_n)) \in \mathbb{R}^{s_n}$. The corresponding codebook entries form the dequantized embeddings at this scale $\hat{z}^{(n)} \in \mathbb{R}^{s_n \times d}$. To enable proper residual updates across different scales, the dequantized embeddings $\hat{z}^{(n)}$ must be restored to a consistent scale. An upsampling operation $\Uparrow(\cdot)$ is applied to bring the embedding scale back to s_N : $\hat{z}^{(n)} = \Uparrow(\hat{z}^{(n)}) \in \mathbb{R}^{s_N \times d}$. This allows the computation of the residual for the next quantization layer: $z^{(n+1)} = z^{(n)} - \hat{z}^{(n)}$.

The downsample-quantize-upsample process is repeated for all N layers, progressively refining the motion representation at different temporal granularities. After N iterations, we obtain the complete multi-scale token set $x = (x^{(1)}, x^{(2)}, \dots, x^{(N)})$ for SAR modeling. The final dequantized embedding \hat{z} fed into the detokenizer for motion reconstruction is computed as the sum of all intermediate upsampled embeddings: $\hat{z} = \sum_{n=1}^N \hat{z}^{(n)}$ (indicated by the addition symbol in Fig. 8). Listing 1 presents the PyTorch-style pseudocode for this forward process.

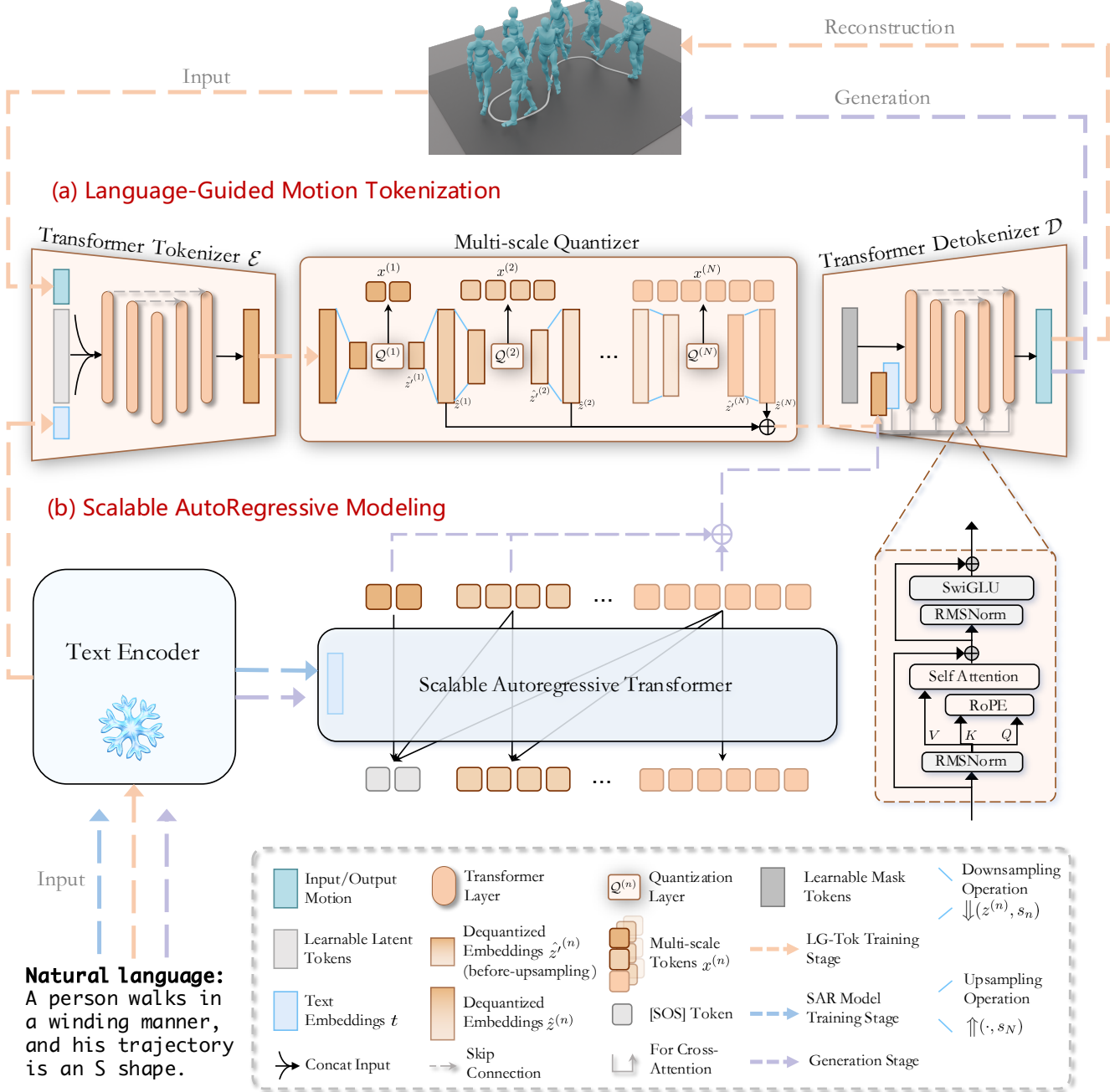


Figure 8. Complete tokenization-generation-detokenization pipeline. (a) *Language-Guided Motion Tokenization*: The transformer tokenizer encodes motion with text guidance, followed by multi-scale quantization that produces multi-scale token sets to enable (b) *Scalable AutoRegressive Modeling*: The SAR model performs scale-by-scale generation conditioned on text, and the transformer detokenizer decodes motion from dequantized embeddings. Orange, blue, and purple dashed lines indicate LG-Tok training, SAR Model training, and generation flows, respectively.

2) SAR Model Training Stage. Leveraging multi-scale tokens, SAR modeling reformulates traditional token-by-token prediction [10] into scale-by-scale generation. The blue dashed line in Fig. 8 illustrates the SAR model training flow. Given input $([\text{sos}], x^{(1)}, x^{(2)}, \dots, x^{(N-1)})$, SAR predicts $(x^{(1)}, x^{(2)}, \dots, x^{(N)})$, where $x^{(n)} = (x_1^{(n)}, \dots, x_{s_n}^{(n)})$ represents the

token sequence at scale s_n (as defined in Eq. 5). The SAR likelihood is defined as:

$$p(x^{(1)}, \dots, x^{(N)} \mid t) = \prod_{n=1}^N p(x^{(n)} \mid x^{(1)}, \dots, x^{(n-1)}, t) \quad (6)$$

where all tokens in $x^{(n)}$ are predicted simultaneously at step n . A scale-wise causal attention mask ensures that each $x^{(n)}$ can only attend to $x^{(\leq n)}$, which makes the generation at each step condition on flattened features from previous scales and text embeddings t (produced by the text encoder). Thanks to scalable autoregressive modeling, the inference steps align with the number of multi-scale quantizer layers N . Following MoSa, we set $N = 10$ in our experiments. This reduces inference from 49 sequential steps (for token-by-token generation) to 10, since SAR predicts all tokens within each scale in parallel at each step. Moreover, the introduction of multi-scale intermediate representations enhances the model’s contextual modeling capability.

3) Generation Stage. With both LG-Tok and the SAR model trained, they can be jointly leveraged to generate high-quality, diverse motions from natural language descriptions. The purple dashed line in Fig. 8 illustrates the complete generation flow, comprising three key phases: autoregressive token generation, dequantization, and motion detokenization. The SAR model first predicts (samples) the first scale’s token sequence $\hat{x}^{(1)}$ in parallel, conditioned on text embedding t extracted by the text encoder. Subsequently, the prediction of tokens $\hat{x}^{(2)}$ at the second scale is conditioned on $(\hat{x}^{(1)}, t)$; the prediction of tokens $\hat{x}^{(3)}$ at the third scale is conditioned on $(\hat{x}^{(1)}, \hat{x}^{(2)}, t)$, This autoregressive process continues iteratively until all N scales are predicted. Then, the predicted multi-scale tokens $(\hat{x}^{(1)}, \dots, \hat{x}^{(N)})$ are processed through dequantization. First, each scale’s tokens are dequantized by getting their corresponding embeddings from the codebook. Following the upsampling and summation operations described in stage 1), these embeddings are combined to form the final dequantized embeddings \hat{z} . Finally, detokenization is performed: the learnable mask tokens in the LG-Tok detokenizer interact with both \hat{z} and text embedding t through separate cross-attention layers to decode the final motion output.

C. Robust Language Guidance: Language-Drop Scheme

While text injection in tokenization shares conceptual similarities with language-guided image tokenizers (e.g., Tex-Tok [70]), our contribution extends beyond direct cross-modal adaptation. The critical innovation lies in the *Language-Drop Scheme* (Sec. 3.4), a training strategy specifically designed to enable robust language-free guidance during detokenization. Table 5 presents comprehensive ablations demonstrating two fundamental advantages: 1) regularization that prevents over-reliance on semantic information, and 2) semantic amplification that enhances text-motion alignment during generation.

Method	Reconstruction			Generation		
	FID \downarrow	Top 1 \uparrow	MM-Dist. \downarrow	FID \downarrow	Top 1 \uparrow	MM-Dist. \downarrow
HumanML3D	LG-Tok ($g = 2.0$)	0.022\pm.000	0.502 \pm .002	3.250 \pm .010	0.057\pm.003	0.542\pm.003
	LG-Tok ($g = 0.0$)				0.061 \pm .003	0.534 \pm .003
	w/o lang-drop scheme	0.039 \pm .000	0.505\pm.002	3.233\pm.009	0.132 \pm .005	0.533 \pm .003
	w/o text guidance	0.025 \pm .000	0.494 \pm .002	3.301 \pm .009	0.062 \pm .002	0.533 \pm .003
Motion-X	LG-Tok ($g = 1.0$)	0.041\pm.001	0.577 \pm .002	3.890 \pm .008	0.088\pm.006	0.582\pm.002
	LG-Tok ($g = 0.0$)				0.139 \pm .008	0.576 \pm .002
	w/o lang-drop scheme	0.057 \pm .002	0.580\pm.002	3.846\pm.007	0.136 \pm .007	0.574 \pm .002
	w/o text guidance	0.090 \pm .002	0.568 \pm .002	4.022 \pm .008	0.257 \pm .010	0.555 \pm .002

Table 5. Ablation study on language-drop scheme and language-free guidance. Symbol g denotes the guidance scale for language-free decoding during generation. “w/o text guidance” represents a vanilla Transformer tokenizer without text injection.

1) Regularization Effect. The language-drop scheme enforces a crucial balance during training: the detokenizer must learn to reconstruct motion from tokens alone during dropout periods (when text is masked), while simultaneously leveraging semantic guidance when text is available. Without this regularization, the detokenizer becomes overly dependent on semantic cues. As shown in Table 5, the “w/o lang-drop scheme” variant suffers severe degradation during generation, even underperforming the vanilla baseline (FID on HumanML3D: 0.057 \rightarrow 0.132). This demonstrates that constant text guidance without proper regularization causes the detokenizer to over-rely on semantic information while neglecting structural details encoded in motion tokens.

2) Semantic Amplification. Beyond regularization, the language-drop scheme enables semantic amplification through language-free guidance during inference: $\hat{m} = (1 + g) \cdot \hat{m}_c - g \cdot \hat{m}_u$, where \hat{m}_c and \hat{m}_u represent motions decoded with and without text conditioning, respectively. The difference term $g \cdot (\hat{m}_c - \hat{m}_u)$ amplifies text-specific features, allowing generated motions to better align with textual descriptions. This mechanism demonstrates substantial improvements: on HumanML3D, guidance ($g = 2.0$) achieves FID of 0.057 versus 0.061 without guidance; on Motion-X, the improvement is more pronounced (0.088 vs. 0.139), demonstrating that language-drop is a fundamental enabler of semantic control during generation.

D. Feature Extractor Training on the Motion-X Dataset

Quantitative evaluation of stochastic generative models has been well-established in the image generation domain. This typically involves extracting high-dimensional features from deep networks (e.g., Inception V3). These high-dimensional features are then used to measure distributional differences, diversity, and other properties. Similarly, quantitative evaluation for text-to-motion generation has been inspired by this paradigm. Guo *et al.* [25] trained separate feature extractors for text and motion using contrastive loss, and subsequent methods have adopted these extractors to evaluate key metrics such as FID and R-Precision. Recently, Meng *et al.* [26] revealed redundancy in data representations and retrained feature extractors on HumanML3D using tighter representations, while also introducing a MotionCLIP-style [31] network architecture for CLIP-based score evaluation. In our experiments, we adopt the HumanML3D feature extractor they provide and use it to reproduce representative methods. Since no feature extractor was provided for the larger Motion-X dataset, we trained a corresponding feature extractor following the discussions by Meng *et al.* in their GitHub issue¹. Notably, we made two reasonable adaptations:

1) Vocabulary handling. We observe that the Motion-X dataset contains a significantly more diverse vocabulary. When using the original vocabulary provided by Guo *et al.*, many out-of-vocabulary words are uniformly marked as `unk` (unknown token), resulting in missing word embeddings. To better preserve and understand semantic information, we use GloVe 6B pre-trained word embeddings and perform part-of-speech tagging directly with spaCy.

2) Batch size adjustment. When training the MotionCLIP-style network for CLIP-based score evaluation, we observe that mini-batch contrastive training (e.g., batch size = 8) results in negligible training loss reduction. This phenomenon likely stems from the inherently high similarity among motion descriptions, causing the negative sample set to contain numerous “false negatives” that are semantically highly related to the anchor description, thereby undermining the learned embeddings [86, 87]. To mitigate this issue, we appropriately increase the batch size during training to enhance negative sample diversity. We ultimately set the batch size to 32 and conduct corresponding ablation studies:

Batch size	CLIP-score
8	0.012
16	0.026
32	0.672
64	0.656
128	0.630

Table 6. Ablation study on batch size for training the MotionCLIP-style CLIP-score evaluator on Motion-X.

E. Details of Baseline Reproduction on the Motion-X Dataset

After training the Motion-X feature extractor, we reproduced representative baselines with extended training for optimal validation performance: StableMoFusion (150K steps vs. 50K original), MotionDiffuse (100 vs. 50 epochs), and MoMask tokenizer (100 vs. 50 epochs), *etc.* Additionally, for tokenizer-based models (both discrete and continuous), we further enhance robustness by training on out-of-distribution (OOD) data. We observe that under the current generation paradigm targeting ~ 10 s of motions (< 200 frames), a substantial number of longer motion sequences (≥ 200 frames) remain unused. We leverage these as OOD data by scanning them with a sliding window of 200 frames for tokenizer training. Notably, in comparison to pre-training followed by fine-tuning, we employ parallel training: each batch comprises 50% OOD samples and 50% in-distribution samples. This prevents catastrophic forgetting while enabling knowledge transfer from extended

¹<https://github.com/neu-vi/MARDM/issues/8>

motion sequences. Table 7 demonstrates the effectiveness of this approach, showing reconstruction improvements for LG-Tok and MoMask’s tokenizer on the Motion-X test set:

Method	R Precision↑			FID↓	MultiModal Dist↓	MPJPE↓
	Top 1	Top 2	Top 3			
MoMask	0.554^{±.002}	0.743^{±.001}	0.829^{±.001}	0.394^{±.005}	4.284^{±.006}	24.9
w/o OOD training	0.540 ^{±.002}	0.727 ^{±.002}	0.813 ^{±.001}	0.427 ^{±.004}	4.482 ^{±.008}	34.1
LG-Tok	0.577^{±.002}	0.773^{±.001}	0.858^{±.001}	0.041^{±.001}	3.890^{±.008}	31.0
w/o OOD training	0.563 ^{±.002}	0.757 ^{±.001}	0.842 ^{±.001}	0.086 ^{±.003}	4.098 ^{±.007}	32.7

Table 7. Training on OOD data improves reconstruction performance for tokenizer-based models on the Motion-X test set.

F. Qualitative Comparison for Text Guidance

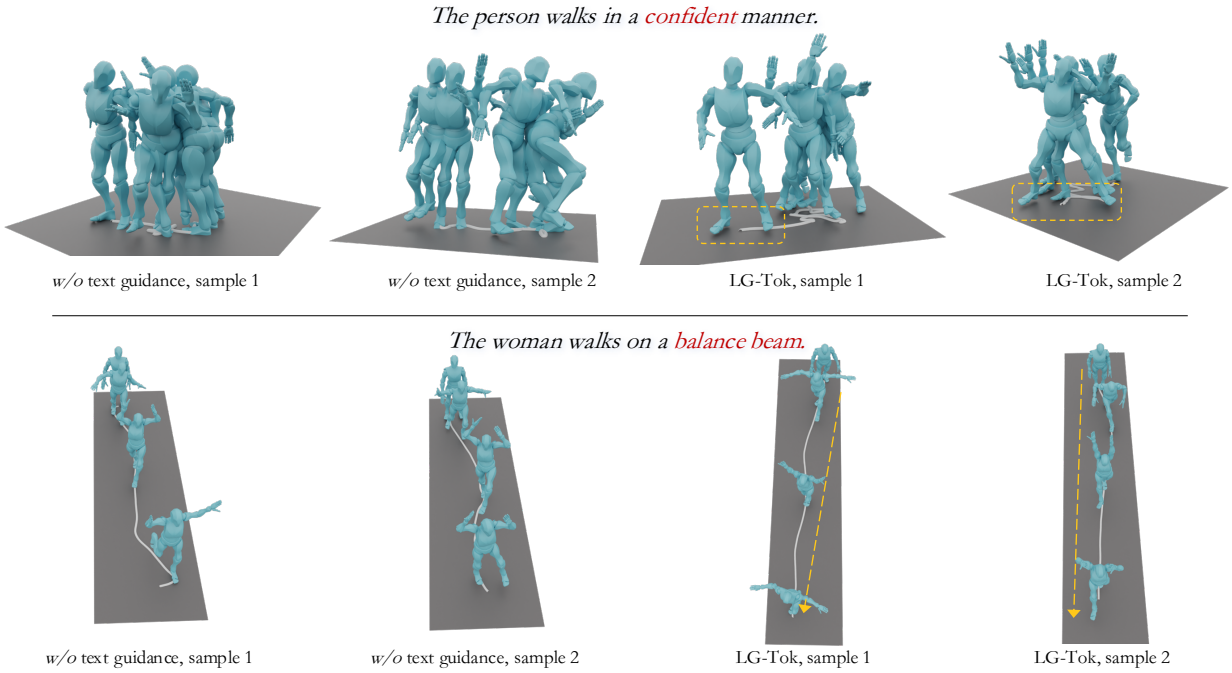
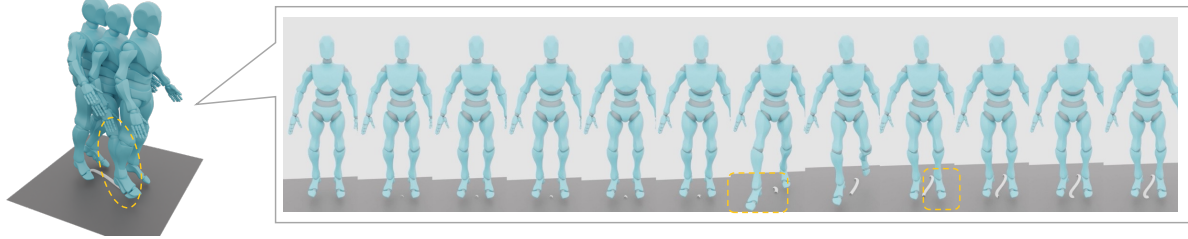


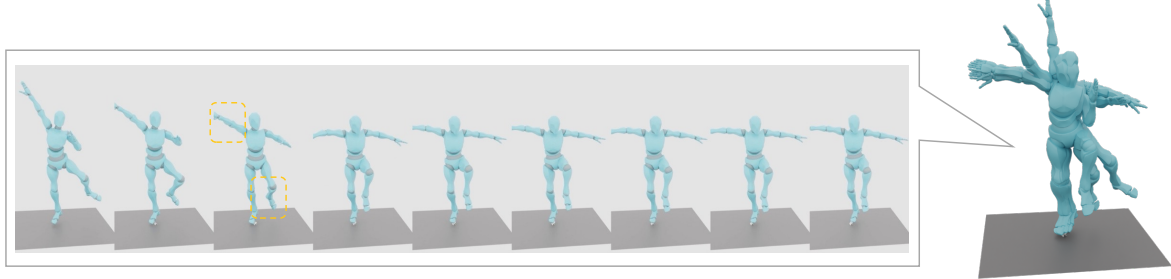
Figure 9. **Qualitative comparison for text guidance.** Qualitative comparison based on Motion-X checkpoint demonstrating that text-guided tokenization (LG-Tok) generates motions with improved semantic alignment to text descriptions compared to training without (w/o) text guidance.

We compare the qualitative results of our transformer-based tokenizer with text guidance (LG-Tok) against the variant without text guidance (w/o text guidance) on the Motion-X dataset. Fig. 9 illustrates two representative examples. We argue that incorporating language guidance enables LG-Tok to capture high-level semantic representations, which better align the generated motions with textual conditions. In the first example (“*The person walks in a confident manner*”), both variants generate walking motions. Yet, the w/o text guidance version exhibits predominantly single-foot movements with noticeable foot-slip artifacts. In contrast, LG-Tok produces bilateral swaying motions that better convey the semantic notion of “confident” walking. In the second example (“*The woman walks on a balance beam*”), LG-Tok generates a nearly straight trajectory, while w/o text guidance version shows slight curvature deviations. These qualitative comparisons demonstrate the advantages of integrating natural language during tokenization. The role of language guidance in the detokenization stage is further analyzed in the next section.

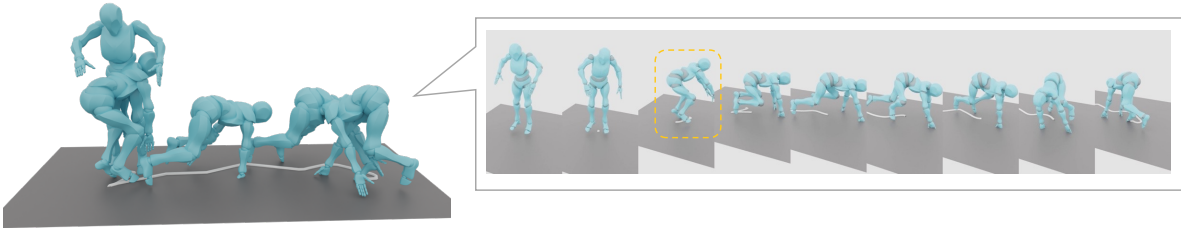
(a) a person takes one step forward with their *right foot* and then with *their left* to end with their feet side by side.



(b) the person is *balancing* on one leg using *his hands* to help balance



(c) a man turns to his left, then *goes down onto a crawl*, moving around on his hands and feet.



(d) a person quickly runs forward and stoops to *pick up an object* before carrying it off.

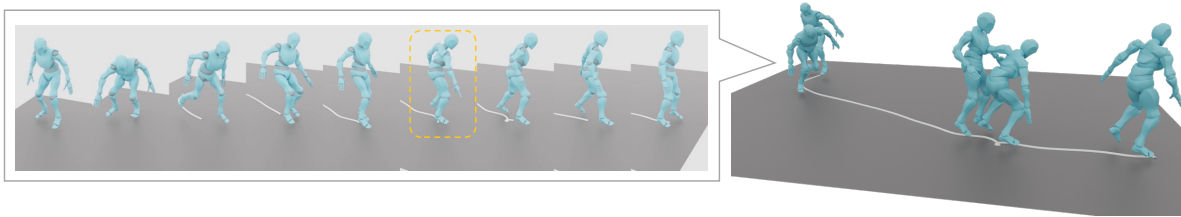


Figure 10. **More qualitative results on HumanML3D.** Each motion sequence is visualized with temporal expansion, with yellow dashed boxes highlighting key frames corresponding to the emphasized actions in the text descriptions (shown in blue and red).

G. The Role of Language Guidance in the Detokenization Stage during Generation

Our language-guided tokenization establishes motion-text alignment during training, enabling the detokenizer to act as a *semantic amplifier* during generation. As shown in Table 8, language-free guidance decoding consistently improves generation quality across both datasets. This phenomenon reveals that language guidance in detokenization serves as a semantic refinement mechanism: the tokens generated by the generative model already encode high-level semantic information learned during tokenization, and the detokenizer’s language conditioning further enhances this semantic coherence. Notably, even in

free-form generation (where the generative model operates without text conditioning), language-free guidance decoding also improves quality (FID: 4.025→3.564 on HumanML3D, 25.093→14.715 on Motion-X), demonstrating that the detokenizer can leverage its learned language-motion alignment to refine arbitrary token sequences semantically. This validates our hypothesis that language guidance in detokenization acts as a continuous semantic enhancement process, translating compact token representations into motion sequences with improved semantic fidelity.

Method	FID ↓		R-Precision Top-1 ↑		CLIP-score ↑	
	HumanML3D	Motion-X	HumanML3D	Motion-X	HumanML3D	Motion-X
Free-form Generation (no text in generative model)						
w/o language decoding	4.025 \pm .094	25.093 \pm .322	0.044 \pm .001	0.048 \pm .001	0.089 \pm .002	0.070 \pm .001
w/ language decoding	3.564\pm.079	14.715\pm.200	0.054\pm.001	0.101\pm.001	0.108\pm.002	0.154\pm.001
Text-conditioned Generation (standard setting)						
w/o language decoding	0.061 \pm .003	0.139 \pm .008	0.534 \pm .003	0.576 \pm .002	0.665 \pm .001	0.680 \pm .000
w/ language decoding	0.057\pm.003	0.088\pm.006	0.542\pm.003	0.582\pm.002	0.669\pm.001	0.682\pm.000

Table 8. Effect of language-free guidance decoding during generation.

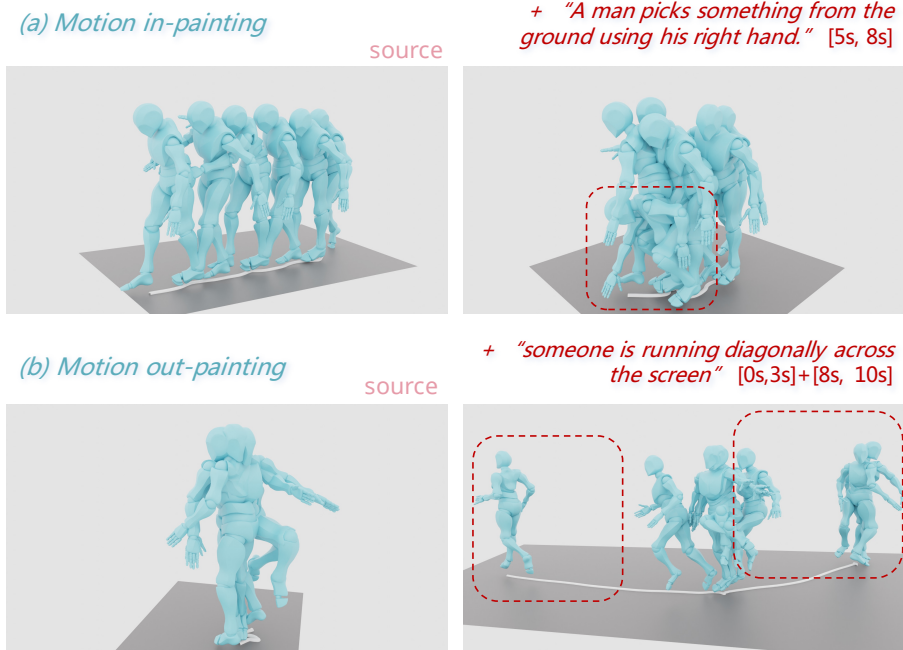


Figure 11. **Motion editing results from LG-Tok.** (a) *Motion in-painting*: given a source motion sequence with overlapping characters (left), our model generates a coherent edited motion where a man bends down and picks something from the ground using his right hand during [5s, 8s] (red dashed box), seamlessly blending with the surrounding context. (b) *Motion out-painting*: starting from a single source character (left), LG-Tok extends the motion temporally and spatially, creating smooth continuations at [0s, 3s] (left red box) and synthesizing dynamic running motions diagonally across the scene at [8s, 10s] (right red box).

H. More Qualitative Results

We generate additional qualitative results using our model trained on HumanML3D to demonstrate the effectiveness of our approach further. As shown in Fig. 10, each human motion is accompanied by a corresponding temporal expansion visualization, with key frames highlighted in yellow dashed boxes to emphasize the critical motion phases described in the text prompts. In example (a), the model accurately captures the sequential stepping motion, with the *right foot* movement clearly visible in the early frames (highlighted) and the subsequent *left foot* action leading to the final pose with *feet side by side*.

Example (b) demonstrates precise control over complex balance motions, where the model generates realistic *balancing* poses on one leg while correctly positioning the *hands* (highlighted) to maintain equilibrium. In example (c), the generated motion faithfully follows the described sequence: the person first *turns to his left*, then smoothly transitions into a crawling position (*goes down onto a crawl*, highlighted), and continues moving on hands and feet. Example (d) showcases the model’s ability to synthesize fine-grained actions, where the person *quickly runs forward*, executes a precise stopping motion, and performs the detailed action of *picking up an object* (highlighted) before carrying it away. These results demonstrate that our language-guided tokenization enables the model to generate motions that are not only semantically aligned with text descriptions but also exhibit smooth temporal transitions and accurate correspondence between linguistic emphasis and motion details.

I. Application: Motion Editing

We provide motion editing results to demonstrate that LG-Tok’s benefits extend beyond standard text-to-motion generation to constrained tasks. Following protocols in prior generative models (*e.g.*, MoSa [23], MoMask [12]), while preserving the inherent editability of the generative model, we can further enhance precise control by applying an edit mask during the *detokenization* stage to enable language guidance only in designated temporal regions. Specifically, given a binary temporal mask $\mathcal{M} \in \{0, 1\}^F$ defining the regions to edit, the detokenizer applies text guidance conditionally:

$$\hat{m} = \mathcal{D}(\hat{m}_l, \hat{z}, t, \mathcal{M}) \quad (7)$$

where mask tokens interact with text embeddings t through cross-attention only in regions where $\mathcal{M} = 1$, while regions with $\mathcal{M} = 0$ rely solely on dequantized embeddings \hat{z} without text conditioning. This enables precise temporal control for partial generation tasks such as motion editing and in-betweening. As illustrated in Fig. 11, our model successfully performs both motion in-painting and out-painting, seamlessly blending edited regions with the surrounding motion context. These results demonstrate LG-Tok’s capability to maintain motion coherence while adapting to diverse text-guided editing scenarios.

J. Evaluation of Average Inference Time

MotionDiffuse [46]	T2M-GPT [10]	MoMask [12]	MMM [11]	StableMoFusion [82]	MoSa [23]	MARDM [26]	LG-Tok (Ours)
4.086s	0.127s	0.062s	0.085s	0.153s	0.045s	2.109s	0.121s

Table 9. Average Inference Time Results Comparison between our method and baseline methods.

To provide a comprehensive evaluation, we assess the computational efficiency of our method in terms of average inference time (AIT). Table 9 reports the efficiency of motion generation over 100 samples on a single Nvidia 4090 device. While LG-Tok achieves superior generation quality across all metrics, it maintains millisecond-scale latency (0.121s), demonstrating an effective balance between generation quality and computational efficiency.

K. Limitations

Unlike convolutional tokenizers (*e.g.*, MoMask with 64-frames window size requiring \sim 2GB memory), LG-Tok’s attention-based architecture with global attention over motion, text, and latent tokens consumes $10\times$ more memory. To mitigate this limitation, we introduce mixed-precision training, which enables tokenizer training on a single 24GB GPU (RTX 4090). However, this increased memory footprint inevitably extends training time: tokenizer training requires approximately 2 days on a single RTX 4090, compared to several hours for convolutional baselines. For inference efficiency analysis, please refer to Sec. J. Despite these computational costs, the substantial quality improvements justify this overhead.

```

1  import torch.nn as nn
2  from torch.nn import functional as F
3
4  class LGTok(nn.Module):
5      def __init__(self, scales=(2, 4, 6, 9, 12, 16, 20, 25, 30, 36), **kwargs):
6          super(LGTok, self).__init__()
7          # The predefined scale scheduler S = (s_1, s_2, ..., s_N)
8          self.scales = scales
9          self.N = len(scales)
10         self.tokenizer = Tokenizer(**kwargs)
11         self.detokenizer = Detokenizer(**kwargs)
12         self.quantizers = nn.ModuleList([Quantizer(**kwargs) for _ in range(self.N)])
13
14     def forward(self, m, t):
15         # Forward pass for the LG-Tok model.
16         # Args: m: input motion, t: natural language
17         # Returns: m_hat: reconstructed motion, x: multi-scale token set
18         z = self.tokenizer(m, t)
19         z_hat, s_N = 0., self.scales[-1]
20         # Eq (5) in paper, multi-scale token set x = (x^(1), x^(2), ..., x^(N))
21         x = []
22
23         # Multi-scale quantization
24         for n in range(self.N):
25             s_n, quantizer = self.scales[n], self.quantizers[n]
26
27             # Perform downsampling and quantization: x^(n) = Q^(n) (downsample(z^(n), s_n))
28             x_n = quantizer(F.interpolate(z, size=(s_n)))
29
30             # Get corresponding codebook entries, form the dequantized embeddings
31             z_prime_hat_n = quantizer.codebook(x_n)
32
33             # Perform upsampling to bring the embedding scale back to s_N
34             z_hat_n = F.interpolate(z_prime_hat_n, size=(s_N))
35
36             # Compute the residual for the next quantization layer
37             z = z - z_hat_n
38             z_hat += z_hat_n # z_hat = sum of all z_hat^(n)
39             x.append(x_n)
40
41         m_hat = self.detokenizer(z_hat, t)
42         return m_hat, x

```

Listing 1. PyTorch-style pseudocode for multi-scale quantization in LG-Tok. The tokenizer encodes motion with text guidance into latent features z . Multi-scale quantization iteratively performs downsample-quantize-upsample operations across N scales, producing multi-scale token set $x = (x^{(1)}, \dots, x^{(N)})$ for SAR training. The final dequantized embeddings $\hat{z} = \sum_{n=1}^N \hat{z}^{(n)}$ are decoded by the detokenizer to reconstruct motion \hat{m} .